



# Lanhushen stimulates the positive cross-regulation mediated by the S1P axis to ameliorate the disorder of glucolipid metabolism induced by the high sucrose diet in *Drosophila melanogaster*

Gengyuan Yu<sup>a,1</sup>, Mo Sun<sup>c,1</sup>, Tonghua Zhang<sup>a</sup>, Haoran Xu<sup>a</sup>, Jiaqi Wang<sup>a</sup>, Wanting Ye<sup>a</sup>, Peng Wang<sup>a</sup>, Shiyun Zhang<sup>a</sup>, Chenning Zhang<sup>b,\*\*</sup>, Yikun Sun<sup>a,\*</sup>

<sup>a</sup> School of Chinese Materia Medica, Beijing University of Chinese Medicine, Beijing 102488, China

<sup>b</sup> Department of Pharmacy, Xiangyang No. 1 People's Hospital Affiliated to Hubei University of Medicine, Xiangyang 441000, China

<sup>c</sup> School of Biological Sciences, Georgia Institute of Technology, Atlanta, GA 30332, USA



## ARTICLE INFO

Handling Editor: Dr. K. Shaari

### Keywords:

Lanhushen

Type 2 diabetes mellitus

*Drosophila melanogaster*

Sphingosine 1-phosphate

## ABSTRACT

**Ethnopharmacological relevance:** Herba Wanlenbergiae, named 'Lanhushen' (LHS) in Chinese, is derived from the dried herba of *Wahlenbergia marginata* (Thunb.) A.DC. It is an abundant resource that has been used in traditional Chinese medicine (TCM) for over 600 years. LHS has the effects of enriching consumptive disease and relieving deficient heat, consistent with the therapy for type 2 diabetes mellitus (T2DM) in TCM. As the basic remedy of Yulan Jiangtang capsules, a listed Chinese medicine specifically for treating T2DM, LHS is a potential candidate for an anti-T2DM drug. However, due to the lack of pharmacodynamic studies and chemical component analysis, the application and development of LHS as a treatment for T2DM have been hindered.

**Aim of the study:** To evaluate the regulation of the disorder of glucolipid metabolism using LHS extracts and its therapeutic potential in T2DM.

**Materials and methods:** Chemical components in LHS extracts were analysed using UPLC-Q Exactive-Orbitrap-MS. Subsequently, high sucrose diet (HSD)-induced *Drosophila melanogaster* were used as suitable models for T2DM in vivo. Behavioural and biochemical tests were performed to evaluate the regulation of the disorder of glucolipid metabolism using LHS in T2DM flies. Furthermore, integrative metabolomic and transcriptomic analysis was applied to reveal the specific effects of LHS extracts on metabolites and genes. Meanwhile, bioinformatic analysis was carried out to predict the targeted transcription factors (TFs) and potentially effective components of LHS extracts.

**Results:** We redefined the chemical profile of LHS with 76 identified chemical components, including 65 chemical components for the first time. As indicated by decreased trehalose, glucose and triglyceride levels and increased total protein levels, LHS extracts were perceived to alleviate the disorder of glucolipid metabolism in HSD-induced T2DM fruit flies. Integrative metabolomic and transcriptomic analysis revealed that LHS extracts eliminated the accumulation of sphingolipids and subsequently stimulated the positive cross-regulation mediated by the sphingosine 1-phosphate (S1P) axis, resulting in the activation of the phosphatidylinositol-3-kinase (PI3K)-protein kinase B (Akt) signalling pathway and inhibition of lysosome-mediated apoptosis. Bioinformatic analysis revealed that the upstream TFs, transcriptional enhancer factor TEF-5 (TEAD3) and peroxisome proliferator-activated receptor alpha (PPARA), were the potential targets of atactylenolide III, dihydrokaempferol and syringaldehyde, the potentially effective components of LHS extracts. Therefore, this TF network was plausibly the basis for the efficacy.

\* Corresponding author. Liangxiang Campus, Beijing University of Chinese Medicine, Yangguang South Street, Liangxiang Higher Education Park, Fangshan District, Beijing 102488, China.

\*\* Corresponding author. Xiangyang No.1 People's Hospital, Hubei University of Medicine, No. 15, Jiefang Road, Fancheng District, Xiangyang 441000, China.

E-mail addresses: [gy0209@163.com](mailto:gy0209@163.com) (G. Yu), [msun330@gatech.edu](mailto:msun330@gatech.edu) (M. Sun), [zonghuaa@163.com](mailto:zonghuaa@163.com) (T. Zhang), [xuhuoran1947@163.com](mailto:xuhuoran1947@163.com) (H. Xu), [m15101049061@163.com](mailto:m15101049061@163.com) (J. Wang), [yewanting0620@163.com](mailto:yewanting0620@163.com) (W. Ye), [18810282691@163.com](mailto:18810282691@163.com) (P. Wang), [20220935151@bucm.edu.cn](mailto:20220935151@bucm.edu.cn) (S. Zhang), [zhangcn1118@163.com](mailto:zhangcn1118@163.com) (C. Zhang), [Sunyk@bucm.edu.cn](mailto:Sunyk@bucm.edu.cn) (Y. Sun).

<sup>1</sup> These authors contributed equally to this work.

**Conclusions:** LHS extracts broadly modulated TF-dependent gene expression and subsequently stimulated the positive cross-regulation mediated by the S1P axis to ameliorate the disorder of glucolipid metabolism. Our study provides critical evidence considering LHS as a potential drug candidate for T2DM, inspiring the discovery and development of innovative therapeutic agents based on the cross-regulation mediated by the S1P axis for treating T2DM and related complications.

## Abbreviations

Akt	protein kinase B	LogP	Log of the octanol/water partition coefficient
ANOVA	analysis of variance	LogS	Log of the aqueous solubility
BPI	base peak intensity	MET	metformin
Caco-2	Caco-2 permeability	NR1H2	oxysterols receptor LXR-beta
Cer	ceramide	OPLS-DA	orthogonal partial least squares discriminant analysis
CL	clearance	PAX3	paired box protein Pax-3
DBD	DNA binding domain	PBS	phosphate buffer solution
DC	docking score	PCA	principal component analysis
DEGs	different expression genes	PDB	Protein Data Bank
dhS1P	dihydrosphingosine 1-phosphate	PI3K	phosphatidylinositol-3-kinase
dhSph	dihydrosphingosine	PPARA	peroxisome proliferator-activated receptor alpha
DM	diabetes mellitus	PPB	plasma protein binding
E75BA	ecdysone-induced protein 75B, isoform A	PRD	segmentation protein paired
ECR	ecdysone receptor	QC	quality control
F <sub>20%</sub>	20% bioavailability	RDC	relative docking score
F <sub>30%</sub>	30% bioavailability	RSD	relative standard deviation
FC	fold change	RXRA	retinoic acid receptor RXR-alpha
FOGX1	forkhead box protein G1	S1P	sphingosine 1-phosphate
Fu	the fraction unbound in plasmas	SCAL	protein scalloped
GluCer	glucosylceramides	SDEGs	significantly different expressed genes
GNAI	G protein alpha i subunit	SEM	standard error of mean
GO	Gene Ontology	SLP1	fork head domain transcription factor slp1
GOMF	GO-molecular function	SLP2	fork head domain transcription factor slp2
GSEA	gene set enrichment analysis	SM	sphingomyelin
HIA	human intestinal absorption	Sph	sphingosine
HSD	high sucrose diet	T <sub>1/2</sub>	half-life period
HSF	heat shock factor protein	T2DM	type 2 diabetes mellitus
HSF1	heat shock factor protein 1	TB	trehalase buffer
IR	insulin resistance	TCM	traditional Chinese medicine
KEGG	Kyoto Encyclopedia of Genes and Genomes	TEAD3	transcriptional enhancer factor TEF-5
LHS	Lanhushen	TFs	transcription factors
LogD	LogP at physiological pH 7.4	USP	protein ultraspiracle
		VDss	volume distribution
		VIP	variable importance in projection

## 1. Introduction

Diabetes mellitus (DM) is gradually becoming an epidemic chronic disease with high incidence among the world. The global diabetes prevalence in 20–79-year-olds in 2021 was estimated to be 10.5% (536.6 million people), rising to 12.2% (783.2 million) by 2045 (Sun et al., 2022). Type 2 diabetes mellitus (T2DM) accounts for 90–95% of all diabetes, which triggers a significant decline in patients' quality of life. As is known to all, T2DM is mainly due to insulin resistance (IR) and deficiency in insulin secretion (American Diabetes Association Professional Practice, 2022). Meanwhile, previous studies have confirmed that T2DM is a multi-factorial chronic disease triggered by several genetic and environmental factors, which is accompanied by metabolic disorders, including hyperglycemia, hyperinsulinemia and hypertriglyceridemia (Xu et al., 2018). Chronic hyperglycemic exposition to tissues and blood vessels increases the risk of developing comorbidities, including retinopathy, nephropathy, neuropathy, stroke, coronary heart disease, etc. (Forbes and Cooper, 2013). Therefore, it is of great significance to find more excellent antidiabetic drugs and clarify their

mechanism.

Since no cure is available, treating patients with T2DM is challenging, but glycaemia and comorbidities can be controlled by pharmacological therapy. However, these anti-T2DM drugs have several side effects that cause a lack of adherence, including episodes of hypoglycaemia, gastrointestinal problems (nausea, vomiting and diarrhoea), oedema and even hepatorenal disorders (Maruthur et al., 2016). Thus, studies on candidates for anti-T2DM drugs focus on various herbal formulas and their extracts to develop hypoglycaemic drugs with low side effects. With the complete system of theories and practical experience for thousands of years, traditional Chinese medicine (TCM) is advisable to guide related research. Herba Wanlenbergiae, named 'Lanhushen' (LHS) in Chinese, is derived from the dried herb *Wahlenbergia marginata* (Thunb.) A.DC. and has been used in TCM for over 600 years. LHS is widely distributed in China's provinces south of the Yangtze River, where the resource is abundant (State Administration of Traditional Chinese Medicine, 1999). According to Herbal Medicines of Southern Yunnan (Lan, 1959), one of the classics of TCM, LHS has the effects of enriching consumptive disease and relieving deficient heat, consistent with the therapy for T2DM in TCM. Of note, with the basic remedy of

LHS, Yulan Jiangtang capsules, a listed Chinese patent medicine specifically for treating T2DM, demonstrated remarkable efficacy in T2DM treatment (Ma et al., 2012). Thereby, LHS should be a potential candidate for anti-T2DM drugs. Nevertheless, due to the lack of pharmacodynamic studies in conjunction with the deficiency of chemical component analysis, the application and development of LHS have been hindered.

Until now, the aetiology of T2DM is currently unclear, while several sphingolipids are proven to be associated with T2DM, such as sphingosine 1-phosphate (S1P), sphingosine (Sph), ceramide (Cer), sphingo-myelin (SM), dihydroosphingosine 1-phosphate (dhS1P), dihydroosphingosine (dhSph), etc. (Chen et al., 2021; Gurgul-Convey, 2022). These metabolites are interconvertible owing to various metabolic enzymes but usually have different functions, constituting the S1P axis and maintaining metabolic homeostasis. Thereinto, active S1P stimulates growth and suppresses apoptosis by activating the phosphatidylinositol-3-kinase (PI3K)-protein kinase B (Akt) signalling pathway. In contrast, Cer and Sph inhibit proliferation and promote lysosome-mediated apoptosis by cathepsin D (Bienias et al., 2016). Hence, the cross-regulation mediated by the S1P axis is reflected in that the relative levels instead of a single metabolite on the S1P axis directly determine the direction of cell and tissue metabolism (He et al., 2021). To date, much has been learned about how the cross-regulation mediated by the S1P axis contributes to cancer progression and treatment (Qiu et al., 2022; Su et al., 2023; Umeshappa et al., 2022). Although there is growing evidence that S1P can improve the adverse effects of IR and reduce apoptosis of islet  $\beta$  cells, while the accumulation of Cer has the opposite effects, the role of the cross-regulation mediated by the S1P axis in treating T2DM has not been reported.

Recently, the fruit fly *Drosophila melanogaster* has emerged as an advantageous alternative to mammalian models for exploring different human pathologies, including metabolism-related disorders such as T2DM (Alvarez-Rendon et al., 2018; Meshrif et al., 2022). It has been demonstrated that the fruit fly exhibits similar metabolic functions as mammals, such as the maintenance of glucose homeostasis, lipid storage and mobilisation and the regulation of food intake (Koyama et al., 2020). Notably, the insulin signalling pathways in the fruit fly are conserved when compared to mammals, which includes the insulin-like peptides and receptor, the insulin receptor substrates, as well as similar downstream components involved in cell growth, cell cycle and protein synthesis control (Garofalo, 2002). A high sucrose diet (HSD) induces a glucolipid metabolism disorder in the fruit fly, which consists of increased trehalose, glucose and triglycerides and is a recognised hallmark of T2DM (Ecker et al., 2017). Consequently, the fruit fly represents an attractive low-cost model for studying T2DM metabolic disorders and potential therapeutic strategies to remedy them.

In the current study, we comprehensively analysed the small molecules in LHS extracts based on UPLC-Q Exactive-Orbitrap-MS, and evaluated the regulatory effects of LHS extracts on the disorder of glucolipid metabolism in a HSD-induced T2DM fruit fly model. Furthermore, the integrative metabolic and transcriptomic analysis revealed that LHS extracts improved disrupted homeostasis of glucolipid metabolism plausibly through the positive cross-regulation mediated by the S1P axis. Finally, bioinformatics technology was used to reveal the potential interaction between core compounds in LHS and key proteins on S1P axis. In brief, current research provide the experimental evidence supporting that LHS may be a novel candidate for anti-T2DM by regulating S1P axis for the first time, which plays an important guiding role in the further development of LHS.

## 2. Materials and methods

### 2.1. Chemicals and reagents

Medicinal materials were obtained from Guizhou Jianxing Pharmaceutical Co. LTD (Guiyang, China) and identified as dry herba of

*Wahlenbergia marginata* (Thunb.) A.DC. by chief pharmacist Zengrong Chang of Beijing Institute for Drug Control. The preparation of LHS extracts was as follows: 50 g of LHS powder was decocted twice with 600 mL and 400 mL deionised water for 1 h and 0.5 h, respectively. The combined extracts were filtered using gauze. Then, 1 mL of extract was centrifuged at 5000 rpm for 10 min, and the supernatant was diluted 10 times with purified water, centrifuged at 12,000 rpm for 10 min, and the supernatant was taken to obtain the sample for MS analysis. The remaining extract was stored at  $-80^{\circ}\text{C}$  for further use.

The total protein, triglyceride, and glucose assay kits were purchased from Nanjing Jiancheng Bioengineering Institute (Nanjing, China). Phosphate buffer solution (PBS, pH 7.4), amylglucosidase and porcine trehalase were purchased from Sigma-Aldrich (Shanghai, China). Trehalose and glycogen were purchased from Shanghai Yuanye Biotechnology Co. LTD (Shanghai, China). Sucrose, agar, Tris, NaCl and KCl were purchased from Beijing Biodee Biotechnology Co. LTD (Beijing, China). Dry yeast was purchased from Oxoid Co. LTD (Hants, UK). Propionic acid was purchased from Beijing Chemical Works (Beijing, China). Metformin (MET) was purchased from Merck Pharmaceutical (Jiangsu) Co. LTD (Nantong, China). Methanol (LC-MS grade), acetonitrile (LC-MS grade) and formic acid (LC-MS grade) were purchased from Thermo Fisher Scientific Co. LTD (Shanghai, China). Ultrapure water was prepared using a Millipore Alpha-Q water purification system (Millipore, Bedford, MA, USA).

### 2.2. UPLC-Q Exactive-Orbitrap-MS conditions

Sample (5  $\mu\text{L}$ ) was injected into a Vanquish Duo UHPLC System for Dual LC Workflows (Thermo Fisher Scientific, MA, USA) with a Waters ACQUITY UPLC BEH C18 column (1.7  $\mu\text{m}$ , 2.1  $\times$  100 mm, Milford, MA, USA) in a column oven at  $40^{\circ}\text{C}$ . The gradient from solvent A (0.1% formic acid aqueous solution) to solvent B (acetonitrile) was performed during 20 min of analysis. The eluting programme was: 5%B for 0–2 min, 5%–95%B for 2–17 min, and 95%B for 18–20 min. The flow rate was set at 0.3 mL/min. MS analysis of the sample was performed on a Q Exactive-Orbitrap-MS (Thermo Fisher Scientific, MA, USA) operated in both positive and negative ion modes equipped with an electrospray ionisation source and nitrogen evaporator N-EVAP 116 (Organonation). Operating parameters were as follows: sheath gas flow rate, 35 arb; auxiliary gas flow rate, 15 arb; capillary temperature,  $350^{\circ}\text{C}$ ; and ion spray voltage, 3.2 kV (+) / 3.0 kV (−). The full scan was used with m/z range of 150–1800 Da. The full scan and ddMS2 resolutions were 70,000 and 17,500, respectively. The identifications were performed using Thermo Xcalibur 3.0 software (Thermo Fisher Scientific, MA, USA).

### 2.3. Potentially effective components prediction

Physicochemical properties, drug-likeness and pharmacokinetic predictions of chemical components identified in LHS extracts were carried out by ADMETlab 2.0 (<https://admetmesh.scbdd.com/>).

### 2.4. Fly strains and husbandry

Wild-type Canton S strains (Institute of Biophysics, Chinese Academy of Sciences) were maintained in an artificial bioclimatic test chamber (Beijing Donglian Har Instrument Manufacturing Co. LTD; SCI400B), with a 12 h–12 h light–dark cycle at  $25^{\circ}\text{C}$  and 60% humidity on a standard diet (54.4 g cornflour, 36 g soybean meal, 4 g agar, 100 g sucrose, 32 g dry yeast, 10 mL propionic acid per litre). All experiments were carried out with newly hatched female flies allowed to mate for 2 days, according to Baenas and Wagner (2022), and followed the regulations of the Animal Care and Use Committee of Beijing University of Chinese Medicine.

## 2.5. Experimental design

Flies were divided into 6 groups and exposed to the different experimental diets as described below: control group (standard diet); model group (standard diet + 200 g sucrose); MET group (standard diet + 200 g sucrose + 0.2% MET); LLHS group (standard diet + 200 g sucrose + 1% LHS extract); MLHS group (standard diet + 200 g sucrose + 2% LHS extract); HLHS group (standard diet + 200 g sucrose + 4% LHS extract). Experiments were initiated by placing 40 flies into vials containing the different diets and repeated with six biological replicates. The flies were subjected to these treatments for 10 days and transferred to vials containing fresh medium every three days.

## 2.6. Flies weight measurement

Ten flies exposed to the different experimental diets were measured for body weight using an electronic balance (Sartorius, Germany; BSA124S). The weight was measured in milligrams and averaged during six independent experiments.

## 2.7. Geotaxis assay

At the end of the different treatment periods, the geotaxis assay was performed to evaluate the locomotor performance of the flies, according to Mishra and Barik (2018), with a few modifications. Briefly, 10 flies from different groups were separately transferred into a measuring cylinder with a cotton plug. After being acclimated to the new environment for 1 min, the flies were tapped at the bottom of the measuring cylinder, and the number of flies that crossed the 16 cm line within 10 s was recorded. The results are expressed as a geotaxis index, the percentage of flies that crossed 16 cm in 10 s during six independent experiments.

## 2.8. Glucose, triglyceride and glycogen measurements

Glucose, triglyceride and glycogen levels of flies from different groups were assessed as described by Tennesen et al. (2014) with a few modifications. Ten flies were rinsed three times with 1 mL cold PBS and homogenised in 200  $\mu$ L cold PBS on ice. Homogenised samples were centrifuged at 2500 rpm at 4 °C for 10 min, and 10  $\mu$ L supernatant was used to measure protein content with a total protein assay kit. Other supernatants were heated for 10 min at 70 °C, and then the triglyceride level was assessed using a triglyceride assay kit. The remaining samples were centrifuged at 13,000 rpm at 4 °C for 3 min, and the supernatants were used for glucose and glycogen assays with a glucose assay kit. The glycogen assay was performed by loading samples in equivalent amyloglucosidase and PBS and incubating them at 37 °C for 60 min. The difference between the absorbance of the amyloglucosidase digested samples and that of the free glucose in the untreated samples was substituted into the glycogen standard curve to calculate the glycogen content. Glucose, triglyceride and glycogen levels were normalised by total protein concentration with six independent experiments.

## 2.9. Trehalose and total protein measurements

Trehalose and total protein levels of flies from different groups were assessed as described by Tennesen et al. (2014) with a few modifications. Ten flies were rinsed three times with 1 mL cold PBS and homogenised in 200  $\mu$ L cold Trehalase buffer (TB) (5 mM Tris pH 6.6, 137 mM NaCl, 2.7 mM KCl) on ice. Homogenised samples were centrifuged at 2500 rpm at 4 °C for 10 min, and 10  $\mu$ L supernatant was used to measure total protein content with a total protein assay kit. Other supernatants were heated for 10 min at 70 °C, then centrifuged at 13,000 rpm at 4 °C for 3 min, and the supernatant was used for the trehalose assay using a glucose assay kit. The trehalose assay was performed by loading samples in equivalent porcine trehalase and TB and incubating them at 37 °C for

24 h. The difference between the absorbance of the porcine trehalase digested samples and that of the free glucose in the untreated samples was substituted into the trehalose standard curve to calculate the trehalose content. Trehalose levels were normalised by total protein concentration with six independent experiments.

## 2.10. Metabolomic analysis

Ten flies of the control group, model group and HLHS group with six biological replicates were each homogenised in 200  $\mu$ L 50% methanol on ice. Homogenised samples were kept at 4 °C for 1 h, then centrifuged at 12,000 rpm at 4 °C for 20 min. The supernatants were taken to obtain the sample for metabolite analysis carried out with six biological replicates. Then, 50  $\mu$ L homogenised samples of each group were vortexed for 3 min and divided into six parallel samples to obtain quality control (QC) samples. The pretreatment of QC samples was the same as above. Six consecutive injections of the same QC sample were initially done in both positive and negative modes to verify the precision of the instrument. Six parallel QC samples were consecutively injected to inspect the method's repeatability. In addition, one QC sample was inserted between six samples for stability.

Metabolite analysis was performed on a UPLC I-Class system coupled with a SYNAPT G2-Si MS system (Waters, Milford, MA, USA). The sample (3  $\mu$ L) was separated on a Waters ACQUITY UPLC BEH C18 column (1.7  $\mu$ m, 2.1 × 100 mm, Milford, MA, USA) in a column oven at 40 °C. A gradient from solvent A (0.1% formic acid aqueous solution) to solvent B (acetonitrile) was performed during 25 min of analysis. The eluting programme was: 5%B for 0–2 min, 5%–60% B for 2–7 min, 77% B for 7–15 min, 77%–98% B for 15–17 min, 98% B for 17–20 min, 98%–5%B for 20–23 min, 5%B for 23–25 min. The flow rate was set at 0.3 mL/min. MS analysis was operated in both positive and negative ion modes equipped with an electrospray ionisation source. The TOF-MS data were acquired in MS<sup>E</sup> centroid mode over the m/z range of 50–1500 Da with a scan rate of 0.2 s. Operating parameters were as follows: source temperature, 100 °C; desolvation gas temperature, 250 °C; desolvation gas flow, 600 L/h; cone gas flow, 50 L/h; capillary voltage, 3.0 kV (+) / 2.5 kV (-); cone voltage, 40 V; transfer MS collision energy, 20–75 eV. The LockSpray containing leucine-enkephalin was infused during data acquisition for online calibration to ensure mass accuracy.

Raw TOF-MS data were processed by Progenesis QI software v 2.3 for peak alignment, peak picking, data normalisation and peak assignments. The resultant data were subjected to principal component analysis (PCA) and orthogonal partial least squares discriminant analysis (OPLS-DA) using MetaboAnalyst 5.0 database (<https://www.metaboanalyst.ca/>) to obtain the clustering information and significant variables expressed as variable importance in projection (VIP) values. Fold change was calculated by normalised data, and p-values were calculated using t-tests. Metabolites with VIP > 1, p < 0.05, and fold change (FC) > 2 / < 0.5 were selected as differential metabolites. Subsequently, the differential metabolites of HLHS group callbacks were selected as the effect biomarkers of LHS, which were identified using the Human Metabolome Databases (<http://www.hmdb.ca/>). R-language packages, including 'Massdatabase', 'ClusterProfiler', 'MetaboAnalystR', 'pheatmap', and 'RColorBrewer', were used for enrichment analysis and visualisation of the identified differential metabolites based on the Kyoto Encyclopedia of Genes and Genomes (KEGG) database.

## 2.11. RNA sequencing

Twenty-five flies of the control group, model group and HLHS group with three biological replicates were homogenised in liquid nitrogen. Total RNA was extracted from the homogenate using TRIzol® Reagent according to the manufacturer's instructions. Then, RNA quality was determined by a 5300 Bioanalyser (Agilent) and quantified using the ND-2000 (NanoDrop Technologies). The RNA sequencing transcriptome library was prepared following Illumina® Stranded mRNA Prep and

Ligation (Illumina, San Diego, CA) using 1 µg of total RNA. Briefly, mRNA was first isolated according to the polyA selection method by oligo(dT) beads and then fragmented by fragmentation buffer. Secondly, double-stranded cDNA was synthesised using a SuperScript double-stranded cDNA synthesis kit (Invitrogen, CA) with random hexamer primers (Illumina). Then, the synthesised cDNA was subjected to end-repair, phosphorylation and 'A' base addition according to Illumina's library construction protocol. Libraries were size selected for cDNA target fragments of 300 bp on 2% Low Range Ultra Agarose followed by PCR amplification using Phusion DNA polymerase for 15 PCR cycles. After being quantified by Qubit 4.0, the paired-end RNA sequencing library was sequenced with the NovaSeq 6000 sequencer ( $2 \times 150$  bp read length). Different expression genes (DEGs) with  $p < 0.05$  and significantly different expressed genes (SDEGs) with  $p < 0.05$  and  $FC > 2/ < 0.5$  between groups were identified according to the transcripts per million reads method. Gene Ontology (GO) and KEGG enrichment analysis of SDEGs were performed by the cluster profile R package. Based on the KEGG dataset, all genes were further analysed by gene set enrichment analysis (GSEA). JASPAR (<http://jaspar.genereg.net/>) was applied for transcription factors (TFs) prediction.

## 2.12. Molecular docking

According to the result of 2.3, syringic acid (PubChem CID: 10742), 2,3-dihydroxybenzoic acid (PubChem CID: 19), 4-methoxysalicylic acid (PubChem CID: 75231), caffeoic acid (PubChem CID: 689043), ferulic acid (PubChem CID: 445858), myristicin (PubChem CID: 4276), syringaldehyde (PubChem CID: 8655), atractylenolide III (PubChem CID: 155948), curcolone (PubChem CID: 101289704) and dihydrokaempferol (PubChem CID: 122850) were used as ligands. The structures of the compounds used as ligands were retrieved from the PubChem database (<https://pubchem.ncbi.nlm.nih.gov/>), processed to minimise energy and transformed into the MOL format as ligands for docking through Chem3D. The X-ray crystal structures of the proteins were obtained from the Protein Data Bank (PDB, <http://www.rcsb.org/>), including oxysterols receptor LXR-beta (NR1H2, PDB ID: 4RAK), retinoic acid receptor RXR-alpha (RXRA, PDB ID: 6FBR), heat shock factor protein 1 (HSF1, PDB ID: 5HDN), paired box protein Pax-3 (PAX3, PDB ID: 3CMY), transcriptional enhancer factor TEF-5 (TEAD3, PDB ID: 7CNL), peroxisome proliferator-activated receptor alpha (PPARA, PDB ID: 6KAX), forkhead box protein G1 (FOXG1, PDB ID: 7CBY). Afterwards, the structures of these proteins were optimised by Maestro 11.8 software, including the assignment of bonds and bond orders, addition of hydrogens, filling in missing loops or side chains, capping uncapped termini, adjusting bonds and formal charges for metals, correcting mislabelled elements, and deleting unnecessary parts in the structure. Subsequently, each grid box was centred on the original ligand in each protein. Visualised docking results and docking score (DC) for each docking were given by Maestro 11.8. The relative docking score (RDC) was calculated as DC (compounds) - DC (corresponding original ligands).

## 2.13. Statistical analysis

Statistical analysis was carried out using SPSS 26.0 one-way analysis of variance (ANOVA) was used to analyse the results, followed by an LSD post hoc test. The  $p$ -value is provided in comparison with the model group and indicated as \* for  $p \leq 0.05$ , \*\* for  $p \leq 0.01$ , \*\*\* for  $p \leq 0.001$ , and \*\*\*\* for  $p \leq 0.0001$ . Data are presented as means  $\pm$  standard error of mean (SEM).

## 3. Results

### 3.1. Chemical components analysis

#### 3.1.1. A total of 76 chemical components were identified in LHS extracts

In the present work, UPLC-Q Exactive-Orbitrap-MS was used to identify the chemical components of LHS, and the base peak intensity (BPI) chromatogram is shown in Fig. 1A and B. In order to ensure the accuracy and reliability of the results to the maximum extent, we not only refer to the secondary mass spectrogram of the database and literature but also identify the main peak and deduce the regular mass spectrometric pattern of each compound (Figs. S1–S11). In total, 76 chemical components were identified in LHS extracts, 65 of which were identified for the first time in LHS (Table 1) and were categorised into 9 classes of natural compounds (Fig. 1B).

#### 3.1.2. Ten chemical components were considered as the potentially effective components based on computational pharmacology

Oral medications must be absorbed by the digestive tract to exert therapeutic effects (Grogan and Preuss, 2023). Consequently, potentially effective component predictions based on computational pharmacology should be followed by chemical component analysis in vitro. It has been suggested that a given compound's low permeability or poor absorption results when it violates one of Lipinski's rule of five (Pathak et al., 2017). Thus, 55 chemical components from LHS extracts confirmed with Lipinski's rule of five according to ADMETlab 2.0 were selected for further screening. Depending on human intestinal absorption (HIA), Caco-2 permeability (Caco-2), 30% bioavailability (F30%) and plasma protein binding (PPB) predicted by ADMETlab 2.0, 10 chemical components that could be potentially absorbed and distributed in the body as prototype components were obtained (Fig. 1C). All of the ten compounds listed in Table 2 exhibited optimal lipophilicity (Optimal:  $0 < \text{Log of the octanol/water partition coefficient } [\text{LogP}] < 3$ ), as well as excellent properties of intestinal absorption (HIA<0.1). Additionally, the values of Caco-2 were in the range from  $-4.42$  to  $-5.61$ , suggesting they had moderate permeability. Thereinto, syringaldehyde, atractylenolide III and curcolone were predicted to show bioavailability at 30%, while the rest presented bioavailability between 20 and 30%, except for dihydrokaempferol and 2,3-dihydroxybenzoic acid. Besides myristicin and curcolone, the PPB values of the rest were optimal. Together, syringic acid, 2,3-dihydroxybenzoic acid, 4-methoxysalicylic acid, caffeoic acid, ferulic acid, myristicin, syringaldehyde, atractylenolide III, curcolone and dihydrokaempferol were considered as the potentially effective components of LHS extracts.

### 3.2. Pharmacodynamic evaluation

#### 3.2.1. LHS extracts improved body weight and climbing ability in flies exposed to high sucrose diets

A HSD significantly changed the morphology of flies and reduced the body weight of flies in comparison with the control group (Fig. 2A and B). Simultaneous exposure to MET and LHS extracts in different concentrations attenuated the effects induced by the HSD. Nevertheless, the beneficial effect of MET and LHS extracts did not reach the control level. In addition, flies exposed to the HSD exhibited a significant decrease in geotaxis index compared to the control group indicating that the climbing ability was diminished (Fig. 2C). The intake of MET and LHS extracts completely reversed the effect of the HSD and even enhanced the climbing ability of flies compared to the control group.

#### 3.2.2. LHS extracts alleviated the disorder of glucolipid metabolism induced by high sucrose diets in flies

A 2.4, 1.8, 2.5 and 1.6-fold increase in whole-body homogenates of trehalose, glucose, glycogen and triglyceride, respectively, was found in flies fed with the HSD compared to the control group (Fig. 2D–G). In turn, the total protein level in whole-body homogenates of flies from the

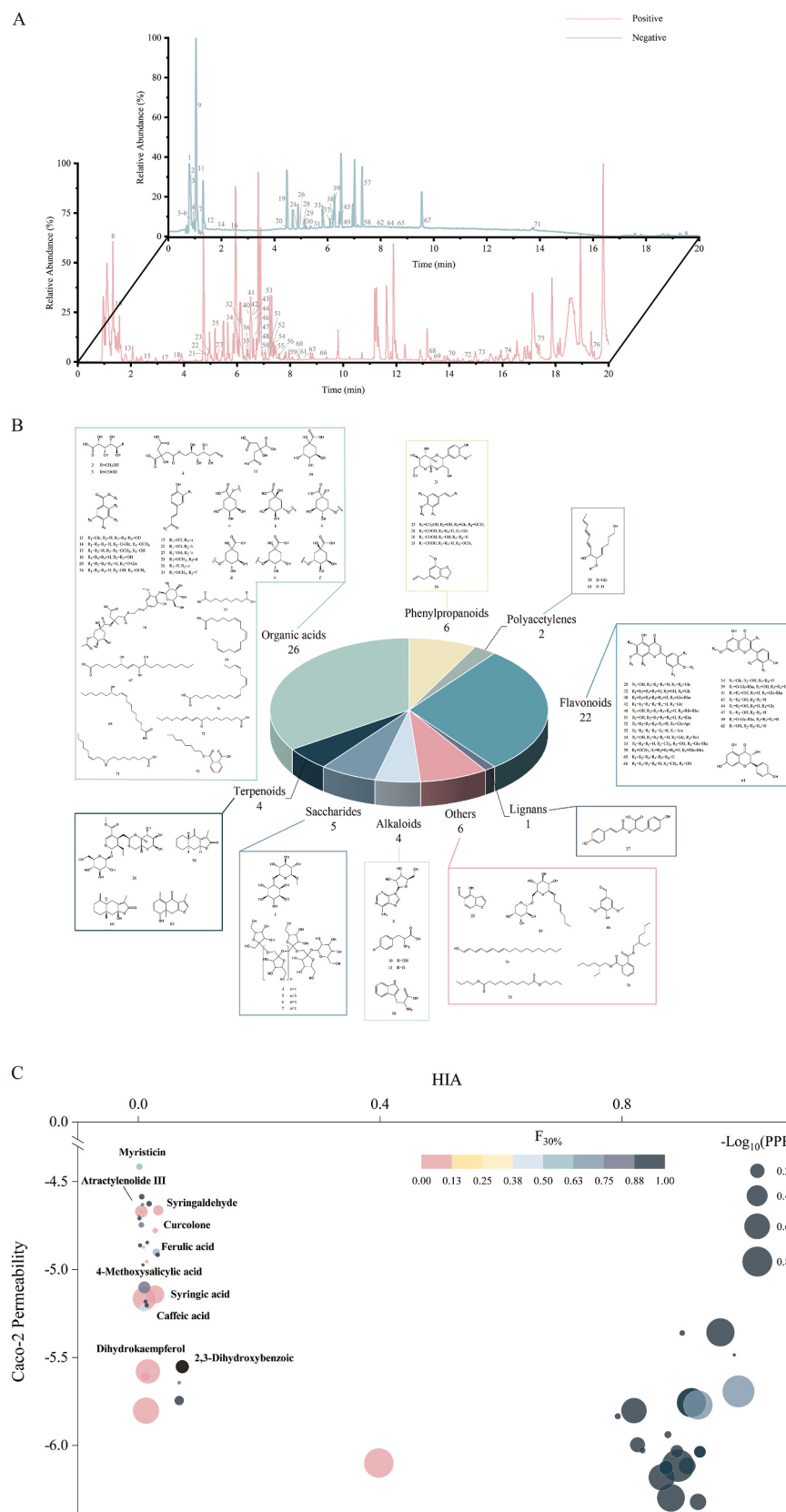


**Fig. 1.** Chemical component analysis of LHS extracts. (A) BPI chromatogram of LHS extracts under positive ion and negative ion modes by UPLC-Q Exactive-Orbitrap-MS. (B) Classification and chemical structures of the 76 identified chemical components. (C) Screening of the potentially effective components based on computational pharmacology.

**Table 1**

Identified chemical components of LHS extracts based on UPLC-Q Exactive-Orbitrap-MS.

NO.	$t_R$ (min)	Theoretical m/z	Measured m/z	Error (ppm)	Ion form	Elemental Composition	MS/MS (m/z)	Identification
1	0.79	341.1089	341.1095	1.75	[M-H] <sup>+</sup>	C <sub>12</sub> H <sub>22</sub> O <sub>11</sub>	89.0245, 85.0296, 59.0139, 101.0245, 113.0246, 129.0196, 165.0409, 267.0725, 71.0139, 341.0737, 119.0351, 179.0566, 161.0461, 297.0840, 221.0670, 143.0356, 147.0297	Glucinol*
2	0.80	195.0510	195.0513	1.15	[M-H] <sup>+</sup>	C <sub>6</sub> H <sub>12</sub> O <sub>7</sub>	195.0513, 75.0088, 129.0196, 87.0089, 59.0139, 99.0089, 177.0408, 89.0246, 85.0296, 159.0300	Gluconic acid*
3	0.81	209.0303	209.0306	1.58	[M-H] <sup>+</sup>	C <sub>6</sub> H <sub>10</sub> O <sub>8</sub>	85.0296, 209.0306, 191.0201, 133.0145, 71.0139, 89.0245, 59.0139, 57.0246, 129.0196, 147.0300, 111.0089, 173.0093	Glucaric acid*
4	0.96	827.2674	827.2718	5.30	[M-H] <sup>+</sup>	C <sub>30</sub> H <sub>52</sub> O <sub>26</sub>	179.0565, 89.0244, 101.0244, 71.0138, 161.0458, 59.0139, 341.1103, 143.0354, 119.0351	1,1,1-Kestopentaose*
5	0.97	1151.3731	1151.3782	4.45	[M-H] <sup>+</sup>	C <sub>42</sub> H <sub>72</sub> O <sub>36</sub>	179.0563, 89.0245, 101.0246, 161.0455, 341.1104, 113.0247, 143.0352, 119.0355, 131.0352, 647.2102, 485.1488, 809.2647	1,1,1,1-Kestoheptaose *
6	0.97	1313.4259	1313.4275	1.23	[M-H] <sup>+</sup>	C <sub>48</sub> H <sub>82</sub> O <sub>41</sub>	179.0565, 101.0245, 161.0458, 341.1081, 113.0247, 1313.4231, 119.0354, 143.0349, 131.0352	Fructo-oligosaccharide DP8/GF7*
7	0.99	989.3202	989.3274	7.24	[M-H] <sup>+</sup>	C <sub>36</sub> H <sub>62</sub> O <sub>31</sub>	179.0564, 89.0245, 101.0245, 71.0139, 161.0453, 113.0245, 341.1099, 119.0353, 143.0353, 131.0353, 485.1523	1,1,1,1-Kestohexaose*
8	1.04	268.1040	268.1036	-1.57	[M+H] <sup>+</sup>	C <sub>10</sub> H <sub>13</sub> N <sub>5</sub> O <sub>4</sub>	136.0623, 268.1046, 89.0236, 57.0340, 73.0287, 119.0356	Adenosine*
9	1.05	353.0725	353.0733	2.04	[M-H] <sup>+</sup>	C <sub>12</sub> H <sub>18</sub> O <sub>12</sub>	85.0296, 209.0306, 191.0201, 161.0459, 111.0090, 99.0453, 147.0302, 57.0346, 129.0196, 71.0138, 87.0088	2-hydroxy-2-[2-oxo-2-[(2R,3R,4S,5R)-2,3,4,5-tetrahydroxy-6-oxohexaoxy]ethyl]butanedioic acid*
10	1.06	182.0812	182.0812	0.11	[M+H] <sup>+</sup>	C <sub>9</sub> H <sub>11</sub> NO <sub>3</sub>	136.0762, 123.0444, 165.0552, 119.0496, 147.0446, 182.0817, 91.0545, 95.0494, 65.0390	Tyrosine*
11	1.07	191.0197	191.0201	1.85	[M-H] <sup>+</sup>	C <sub>6</sub> H <sub>8</sub> O <sub>7</sub>	111.0089, 87.0089, 85.0296, 191.0201, 129.0196, 57.0346, 173.0096, 130.9987, 67.0189, 147.0318	Citric acid*
12	1.24	331.0671	331.0682	3.44	[M-H] <sup>+</sup>	C <sub>13</sub> H <sub>16</sub> O <sub>10</sub>	331.0675, 125.0247, 151.0038, 169.0145, 175.0037, 193.0145, 83.0139, 129.0199, 211.0249, 147.0300, 71.0141	[(2S,3R,4R,5S,6R)-3,4,5-trihydroxy-6-(hydroxymethyl)oxan-2-yl] 3,4,5-trihydroxybenzoate*
13	1.82	166.0863	166.0865	1.23	[M+H] <sup>+</sup>	C <sub>9</sub> H <sub>11</sub> NO <sub>2</sub>	120.0811, 103.0545, 131.0495, 166.0866, 149.0601, 107.0494, 93.0701	Phenylalanine*
14	1.93	329.0878	329.0888	3.14	[M-H] <sup>+</sup>	C <sub>14</sub> H <sub>18</sub> O <sub>9</sub>	167.0353, 123.0456, 108.0219, 152.0117, 149.0246, 121.0307	4-Methoxy-3-[3,4,5-trihydroxy-6-(hydroxymethyl)oxan-2-yl]oxybenzoic acid*
15	2.46	199.0601	199.0601	0.10	[M+H] <sup>+</sup>	C <sub>9</sub> H <sub>10</sub> O <sub>5</sub>	140.0472, 95.0494, 155.0707, 123.0444, 181.0860, 137.0601, 199.0599, 139.0761, 167.0344	Syringic acid*
16	2.49	153.0193	153.0197	2.47	[M-H] <sup>+</sup>	C <sub>7</sub> H <sub>6</sub> O <sub>4</sub>	109.0297, 153.0196, 110.0329, 108.0220, 81.0346, 91.0190	2,3-Dihydroxybenzoic acid*
17	3.09	355.1024	355.1020	-1.12	[M+H] <sup>+</sup>	C <sub>16</sub> H <sub>18</sub> O <sub>9</sub>	163.0394, 91.0576, 145.0289, 135.0444, 117.0336	1-Caffeoylquinic acid*
18	3.66	205.0972	205.0971	-0.51	[M+H] <sup>+</sup>	C <sub>11</sub> H <sub>12</sub> N <sub>2</sub> O <sub>2</sub>	188.0712, 146.0605, 144.0812, 118.0655, 159.0924, 132.0813, 170.0609	Tryptophan*
19	4.45	191.0561	191.0564	1.35	[M-H] <sup>+</sup>	C <sub>7</sub> H <sub>12</sub> O <sub>6</sub>	191.0564, 85.0296, 127.0203, 93.0347, 87.0088, 173.0458, 111.0090, 59.0139, 71.0138	Quinic acid*
20	4.59	299.0772	299.0779	2.34	[M-H] <sup>+</sup>	C <sub>13</sub> H <sub>16</sub> O <sub>8</sub>	137.0246, 93.0347	4-Hydroxybenzoic acid glucoside*
21	4.70	359.1337	359.1333	-1.08	[M+H] <sup>+</sup>	C <sub>16</sub> H <sub>22</sub> O <sub>9</sub>	197.0816, 147.0446, 119.0496, 179.0709, 153.0552, 85.0287, 135.0445, 167.0708, 91.0545, 55.0184, 97.0288, 127.0396, 161.0607, 95.0495, 145.0499	Junipetrioloside A*
22	4.73	355.1024	355.1019	-1.21	[M+H] <sup>+</sup>	C <sub>16</sub> H <sub>18</sub> O <sub>9</sub>	163.0395, 145.0290, 135.0446, 91.0577, 117.0337, 89.0389, 107.0494, 95.0492, 181.0499	Chlorogenic acid*
23	4.75	163.0390	163.0389	-0.56	[M+H] <sup>+</sup>	C <sub>9</sub> H <sub>6</sub> O <sub>3</sub>	163.0395, 135.0445, 145.0289, 117.0339, 89.0389, 107.0495, 79.0545, 73.0287, 63.0235, 53.0391	4-Hydroxy-1-benzofuran-5-carbaldehyde*
24	4.85	167.0350	167.0354	2.62	[M-H] <sup>+</sup>	C <sub>8</sub> H <sub>8</sub> O <sub>4</sub>	152.0118, 167.0352, 153.0151, 124.0165, 123.0455, 108.0218	4-Methoxysalicylic acid*
25	4.89	359.1337	359.1328	-2.36	[M+H] <sup>+</sup>	C <sub>16</sub> H <sub>22</sub> O <sub>9</sub>	141.0551, 147.0446, 109.0288, 179.0709, 85.0287, 57.0340, 126.0316, 119.0496, 97.0287, 81.0338, 161.0600, 145.0502, 197.0820	Demethylsyringin
26	4.97	325.0929	325.0937	2.55	[M-H] <sup>+</sup>	C <sub>15</sub> H <sub>18</sub> O <sub>8</sub>	163.0403, 119.0504, 89.0244, 59.0137, 71.0136	4-O-beta-D-glucosyl-4-coumaric acid*

(continued on next page)

**Table 1 (continued)**

NO.	t <sub>R</sub> (min)	Theoretical m/z	Measured m/z	Error (ppm)	Ion form	Elemental Composition	MS/MS (m/z)	Identification
27	4.98	355.1024	355.1019	-1.21	[M+H] <sup>+</sup>	C <sub>16</sub> H <sub>18</sub> O <sub>9</sub>	163.0395, 145.0290, 135.0445, 91.0576, 117.0337, 89.0387, 107.0498	Neochlorogenic acid*
28	5.03	367.1035	367.1045	2.90	[M-H] <sup>-</sup>	C <sub>17</sub> H <sub>20</sub> O <sub>9</sub>	193.0508, 134.0376, 149.0610, 173.0458, 117.0347, 191.0568, 155.0353, 111.0454, 93.0347, 137.0246, 87.0089	5-O-Feruloylquinic acid*
29	5.05	609.1461	609.1484	3.83	[M-H] <sup>-</sup>	C <sub>27</sub> H <sub>30</sub> O <sub>16</sub>	327.0516, 357.0621, 447.0942, 297.0407, 285.0407, 429.0839, 369.0640, 339.0512, 299.0567	Orientin 4'-O-beta-D-glucopyranoside*
30	5.10	179.0350	179.0355	2.61	[M-H] <sup>-</sup>	C <sub>9</sub> H <sub>8</sub> O <sub>4</sub>	135.0454, 179.0352, 136.0487, 134.0377, 107.0503, 89.0246, 117.0348	Caffeic acid*
31	5.50	337.0929	337.0939	2.91	[M-H] <sup>-</sup>	C <sub>16</sub> H <sub>18</sub> O <sub>8</sub>	191.0564, 93.0347, 163.0404, 173.0458, 87.0088, 119.0504, 111.0454, 67.0190, 145.0298	p-Coumaroylquinic acid*
32	5.83	449.1078	449.1072	-1.53	[M+H] <sup>+</sup>	C <sub>21</sub> H <sub>20</sub> O <sub>11</sub>	299.0555, 329.06613, 353.0661, 395.0771, 325.0710, 413.0875, 287.0552, 165.0192, 137.0241, 85.0288	Orientin*
33	5.85	367.1035	367.1042	1.92	[M-H] <sup>-</sup>	C <sub>17</sub> H <sub>20</sub> O <sub>9</sub>	173.0458, 191.0564, 93.0347, 193.0508, 134.0376, 111.0454, 87.0088, 155.0352, 67.0190, 137.0246, 149.0609, 117.0349	3-O-Feruloylquinic acid*
34	6.01	449.1078	449.1076	-0.53	[M+H] <sup>+</sup>	C <sub>21</sub> H <sub>20</sub> O <sub>11</sub>	329.0660, 449.1778, 299.0557, 413.0885, 353.0659, 151.0758, 431.0986, 383.0757, 287.0554, 161.0608, 137.0237	2-(3,4-Dihydroxyphenyl)-5,7-dihydroxy-3-[3,4,5-trihydroxy-6-(hydroxymethyl)oxan-2-yl]chromen-4-one*
35	6.07	195.0652	195.0653	0.59	[M+H] <sup>+</sup>	C <sub>10</sub> H <sub>10</sub> O <sub>4</sub>	177.0552, 149.0602, 103.0546, 55.0184, 163.0396, 195.0658, 131.0496, 135.0445, 145.0289, 107.0495, 117.0338	Ferulic acid*
36	6.16	193.0859	193.0860	0.31	[M+H] <sup>+</sup>	C <sub>11</sub> H <sub>12</sub> O <sub>3</sub>	161.0602, 133.0653, 105.0702, 193.0862, 115.0546, 135.0809, 91.0545, 103.0546, 79.0545, 165.0911	Myristicin
37	6.16	327.0874	327.0883	2.59	[M-H] <sup>-</sup>	C <sub>18</sub> H <sub>16</sub> O <sub>6</sub>	163.0403, 119.0504, 283.0980, 327.0880, 239.1074, 132.0583, 93.0346, 211.0764, 221.0764, 221.0969, 145.0664	2-o-(4-Coumaroyl)-3-(4-hydroxyphenyl)lactic acid*
38	6.20	549.1825	549.1833	1.45	[M-H] <sup>-</sup>	C <sub>23</sub> H <sub>34</sub> O <sub>15</sub>	179.0716, 341.1246, 164.0481, 85.0295	3-Methoxy-5beta-vinyl-6alpha-(6-O-alpha-D-glucopyranosyl-beta-D-glucopyranosyloxy)-4,4alpha,5,6-tetrahydro-1H,3H-pyran-1-one*
39	6.21	609.1461	609.1476	2.52	[M-H] <sup>-</sup>	C <sub>27</sub> H <sub>30</sub> O <sub>16</sub>	300.0277, 609.1466, 271.0250, 255.0302, 151.0042, 178.9988, 343.0468, 243.0299	Rutin
40	6.21	579.1708	579.1700	-1.47	[M+H] <sup>+</sup>	C <sub>27</sub> H <sub>30</sub> O <sub>14</sub>	313.0710, 283.0605, 337.0711, 85.0287, 71.0494, 367.0816, 379.0818, 397.0926, 415.1032, 309.0758, 323.0917, 433.1141, 271.0605, 129.0550, 147.0661	6-[4,5-Dihydroxy-6-(hydroxymethyl)-3-(3,4,5-trihydroxy-6-methyloxan-2-yl)oxyan-2-yl]-5,7-dihydroxy-2-(4-hydroxyphenyl)chromen-4-one
41	6.23	611.1607	611.1592	-2.33	[M+H] <sup>+</sup>	C <sub>27</sub> H <sub>30</sub> O <sub>16</sub>	303.0505, 85.0286, 71.0495, 129.0552, 61.0288	Quercetin-7-O-rutinoside*
42	6.24	433.1129	433.1122	-1.65	[M+H] <sup>+</sup>	C <sub>21</sub> H <sub>20</sub> O <sub>10</sub>	283.0607, 313.0712, 337.0712, 323.0919, 349.0716, 379.0822, 397.0391, 367.0820, 295.0606, 271.0607, 415.1039, 267.0664, 85.0286, 121.0288, 165.0195	Isovitexin
43	6.25	303.0510	303.0489	-7.05	[M+H] <sup>+</sup>	C <sub>15</sub> H <sub>11</sub> O <sub>7</sub>	303.0504, 229.0501, 257.0542, 153.0187, 137.0239, 165.0189, 285.0397, 201.0553, 183.0299, 247.0606, 121.0287, 149.0239, 109.0287, 68.9974, 195.0293	Morin*
44	6.26	465.1028	465.1022	-1.12	[M+H] <sup>+</sup>	C <sub>21</sub> H <sub>20</sub> O <sub>12</sub>	303.0504, 85.0287, 97.0287, 69.0338, 127.0393, 145.0499, 229.0505, 257.0449, 285.0393, 109.0288, 137.0238, 153.0188, 165.0188, 201.0553, 247.0611, 275.0548	Quercimeritrin
45	6.33	393.1766	393.1776	2.59	[M-H] <sup>-</sup>	C <sub>17</sub> H <sub>30</sub> O <sub>10</sub>	101.0246, 89.0245, 71.0139, 59.0139, 261.1344, 131.0353, 113.0246, 85.0296, 149.0459, 161.0459, 119.0352, 191.0567, 143.0355, 233.0667, 99.0822	(E)-2-Hexenyl 6-O-alpha-L-arabinopyranosyl-beta-D-glucopyranoside*
46	6.33	183.0652	183.0650	-0.85	[M+H] <sup>+</sup>	C <sub>9</sub> H <sub>10</sub> O <sub>4</sub>	123.0445, 95.0495, 140.0473, 155.0709, 183.0657, 53.0391, 127.0758, 67.0546, 105.0452, 97.0650, 81.0338	Syringaldehyde*
47	6.44	303.0499	303.0492	-2.54	[M+H] <sup>+</sup>	C <sub>15</sub> H <sub>10</sub> O <sub>7</sub>	303.0504, 229.0501, 257.0542, 137.0238, 153.0188, 165.0188, 285.0398, 201.0553, 183.0296, 247.0606, 121.0287, 109.0288, 68.9976, 149.0239, 195.0304	Quercetin
48	6.49	565.1552	565.1541	-2.00	[M+H] <sup>+</sup>	C <sub>26</sub> H <sub>28</sub> O <sub>14</sub>	383.0769, 353.0662, 299.0555, 329.0661, 85.0287, 71.0495, 365.0662, 419.0985, 401.0877, 287.0551, 137.0238, 165.0194, 147.0652	Kurilensin A*
49	6.66	593.1512	593.1533	3.48	[M-H] <sup>-</sup>	C <sub>27</sub> H <sub>30</sub> O <sub>15</sub>	285.0405, 284.0372, 593.1502, 89.0244, 149.0457, 255.0300, 101.0245, 85.0295, 71.0138, 59.0138, 227.0352, 113.0247,	Kaempferol 3-O-neohesperidoside*

(continued on next page)

**Table 1 (continued)**

NO.	t <sub>R</sub> (min)	Theoretical m/z	Measured m/z	Error (ppm)	Ion form	Elemental Composition	MS/MS (m/z)	Identification
50	6.72	736.2659	736.2664	0.69	[M + NH <sub>4</sub> ] <sup>+</sup>	C <sub>31</sub> H <sub>42</sub> O <sub>19</sub>	191.0562, 229.0503, 131.0350, 327.0511, 257.0469 147.0446, 179.0709, 119.0497, 161.0603, 133.0654, 127.0395, 193.0714, 91.0545, 129.0556, 301.0923, 95.0495, 85.0288	Wahlenoside B
51	6.80	433.1129	433.1132	0.55	[M+H] <sup>+</sup>	C <sub>21</sub> H <sub>20</sub> O <sub>10</sub>	329.0663, 379.0823, 299.0556, 397.0934, 353.0657, 351.0875, 69.0340, 325.0694, 311.0555, 127.0398, 297.0776, 181.0508, 109.0288, 337.0729, 313.0711, 137.0236, 287.0560, 283.0611	6-C-Fucosylluteolin*
52	6.86	565.1552	565.1562	1.78	[M+H] <sup>+</sup>	C <sub>26</sub> H <sub>28</sub> O <sub>14</sub>	271.0608, 85.0285, 147.0449, 299.0547, 284.0649, 329.0634, 353.0665	Apiin
53	6.95	403.1024	403.1016	-1.83	[M+H] <sup>+</sup>	C <sub>20</sub> H <sub>18</sub> O <sub>9</sub>	283.0606, 367.0819, 337.0711, 313.0712, 349.0713, 321.0763, 309.0763, 297.0763, 295.0606, 121.0287, 271.0613, 281.0807, 267.0659, 163.0392, 201.0548, 229.0508, 97.0286	Isomollupentin*
54	6.97	579.1708	579.1704	-0.83	[M+H] <sup>+</sup>	C <sub>27</sub> H <sub>30</sub> O <sub>14</sub>	337.0713, 299.0557, 313.0710, 399.1086, 381.0978, 355.0817, 343.0825, 287.0554, 325.0714, 417.1191, 561.1622, 517.1343, 475.1237, 449.1108	Farobin B
55	6.99	609.1814	609.1805	-1.41	[M+H] <sup>+</sup>	C <sub>28</sub> H <sub>32</sub> O <sub>15</sub>	301.0712, 286.0480, 85.0287, 71.0495, 463.1253, 129.0549, 147.0667	Diosmin*
56	7.21	233.1536	233.1535	-0.33	[M+H] <sup>+</sup>	C <sub>15</sub> H <sub>20</sub> O <sub>2</sub>	175.1125, 233.1540, 105.0702, 215.1439, 157.1019, 135.0810, 173.1332, 145.1016, 107.0858, 81.0702, 93.0702, 131.0862, 119.0859, 187.1488, 189.1280, 71.0493	Atractylenolide-II*
57	7.29	187.0976	187.0978	1.22	[M-H] <sup>-</sup>	C <sub>9</sub> H <sub>16</sub> O <sub>4</sub>	125.0974, 187.0978, 97.0660, 169.0873, 123.0819, 143.1080, 95.0505	Azelaic acid*
58	7.43	441.1766	441.1780	3.08	[M + COOH] <sup>+</sup>	C <sub>20</sub> H <sub>28</sub> O <sub>8</sub>	143.0714, 89.0248, 59.0139, 71.0139, 185.0969, 101.0247, 159.0824, 119.0353, 125.0606, 113.0248, 215.1084	Lobetyolin
59	7.81	593.1865	593.1868	0.49	[M+H] <sup>+</sup>	C <sub>28</sub> H <sub>32</sub> O <sub>14</sub>	411.1085, 367.0819, 343.0822, 393.0982, 85.0287, 313.0714, 71.0495, 447.1302, 339.0866, 429.1194, 365.1032, 325.0714, 151.0396, 301.0711, 129.0551, 109.0649	ax-4"-Hydroxy-3-'-methoxymaysin*
60	7.90	249.1485	249.1484	-0.41	[M+H] <sup>+</sup>	C <sub>15</sub> H <sub>20</sub> O <sub>3</sub>	145.1017, 131.0860, 191.1073, 171.1173, 173.0967, 231.1387, 99.0443, 189.1283, 249.1487, 143.0862, 213.1287, 185.1340, 161.0969, 105.0703, 119.0861, 93.0701, 81.0702, 71.0494	Atractylenolide III*
61	8.06	235.1329	235.1327	-0.64	[M+H] <sup>+</sup>	C <sub>14</sub> H <sub>18</sub> O <sub>3</sub>	235.1342, 109.0652, 189.0918, 81.0701, 217.1236, 105.0703, 93.0703, 119.0859, 175.1127, 133.1019, 79.0547, 121.0652, 147.1176, 199.1128, 91.0545, 67.0546, 55.0547	Lobetylol*
62	8.12	285.0405	285.0408	1.29	[M-H] <sup>-</sup>	C <sub>15</sub> H <sub>10</sub> O <sub>6</sub>	285.0406, 133.0297, 151.0038, 175.0403, 199.0404, 107.0141, 217.0506, 241.0510, 257.0450	Kaempferol*
63	8.13	247.1329	247.1326	-0.93	[M+H] <sup>+</sup>	C <sub>15</sub> H <sub>18</sub> O <sub>3</sub>	187.1122, 201.1280, 247.1331, 173.1330, 229.1228, 191.0708, 159.1175, 163.0761, 121.0653, 135.0808, 109.0287, 149.0969, 69.0338, 83.0493, 119.0860, 105.0702	Curcolone*
64	8.14	287.0561	287.0565	1.21	[M-H] <sup>-</sup>	C <sub>15</sub> H <sub>12</sub> O <sub>6</sub>	151.0039, 135.0454, 107.0140, 287.0476, 125.0244, 83.0139, 65.0033	Dihydrokaempferol*
65	8.85	269.0455	269.0459	1.31	[M-H] <sup>-</sup>	C <sub>15</sub> H <sub>10</sub> O <sub>5</sub>	269.0457, 149.0243, 117.0349, 151.0037, 121.0294, 225.0552	Apigenin*
66	9.03	301.0707	301.0702	-1.68	[M+H] <sup>+</sup>	C <sub>16</sub> H <sub>12</sub> O <sub>6</sub>	301.0713, 286.0479, 258.0541, 93.0708, 107.0495, 79.0547	Diosmetin*
67	9.58	329.2333	329.2339	1.56	[M-H] <sup>-</sup>	C <sub>18</sub> H <sub>34</sub> O <sub>5</sub>	329.2337, 211.1342, 229.1447, 171.1029, 99.0817, 139.1133, 183.1393, 127.1130, 311.2223, 293.2129, 193.1231	(E)-6,9,10-trihydroxyoctadec-7-enoic acid*
68	13.06	277.2162	277.2157	-1.94	[M+H] <sup>+</sup>	C <sub>18</sub> H <sub>28</sub> O <sub>2</sub>	93.0702, 121.1015, 135.1173, 107.0859, 79.0545, 277.2163, 81.0701, 149.1330, 67.0546, 55.0547, 163.1487, 235.1706, 221.1549, 185.1328, 259.2065, 207.1394	Stearidonic acid*
69	13.09	299.2581	299.2574	-2.28	[M+H] <sup>+</sup>	C <sub>18</sub> H <sub>34</sub> O <sub>3</sub>	71.0859, 81.0702, 57.0704, 95.0858, 141.1278, 97.1017, 155.1443, 109.1021, 123.1173, 133.1013, 161.1334, 245.2259, 263.2356, 253.2540	Ricinoleic acid*
70	13.84	279.2319	279.2313	-1.92	[M+H] <sup>+</sup>	C <sub>18</sub> H <sub>30</sub> O <sub>2</sub>	81.0701, 95.0858, 67.0546, 109.1015, 123.1172, 137.1330, 279.2321, 173.1331, 55.0547, 149.1327, 209.1541, 223.1693, 261.2213, 243.2107	Linolenic acid*

(continued on next page)

**Table 1 (continued)**

NO.	$t_R$ (min)	Theoretical m/z	Measured m/z	Error (ppm)	Ion form	Elemental Composition	MS/MS (m/z)	Identification
71	13.87	295.2279	295.2285	1.97	[M-H] <sup>+</sup>	C <sub>18</sub> H <sub>32</sub> O <sub>3</sub>	295.2281, 277.2174, 171.1029, 183.1027, 195.1392, 59.0138, 125.0975, 99.0812, 141.1280	Coronaric acid*
72	14.50	295.2268	295.2262	-1.83	[M+H] <sup>+</sup>	C <sub>18</sub> H <sub>30</sub> O <sub>3</sub>	151.1124, 277.2168, 67.0546, 69.0702, 95.0495, 93.0702, 81.0702, 107.0859, 79.0546, 161.1331, 133.1017, 105.0703, 55.0548, 147.1175, 125.0967, 241.1956	9-Oxoctadeca-10,12-dienoic acid*
73	14.75	279.1591	279.1584	-2.38	[M+H] <sup>+</sup>	C <sub>16</sub> H <sub>22</sub> O <sub>4</sub>	149.0238, 57.0704, 167.0347, 95.0858, 81.0700, 67.0545, 121.0289	Octyl hydrogen phthalate*
74	15.91	263.2369	263.2363	-2.33	[M+H] <sup>+</sup>	C <sub>18</sub> H <sub>30</sub> O	95.0859, 81.0702, 67.0546, 263.2375, 109.1016, 123.1174, 245.2269, 133.1014, 93.0700, 83.0858, 57.0705, 147.1176, 55.0547, 69.0702, 79.0544, 161.1332, 175.1489	Octadeca-1,3,5,7-tetraen-1-OL*
75	16.96	315.2530	315.2524	-2.02	[M+H] <sup>+</sup>	C <sub>18</sub> H <sub>34</sub> O <sub>4</sub>	139.1123, 203.1285, 121.1016, 69.0703, 81.0702, 97.1016, 93.0704, 149.0967, 157.1226, 57.0704, 111.1172, 259.1912, 167.1074, 131.0860	Dibutyl sebacate*
76	19.09	391.2843	391.2838	-1.22	[M+H] <sup>+</sup>	C <sub>24</sub> H <sub>38</sub> O <sub>4</sub>	149.0238, 71.0858, 57.0704, 167.0345, 89.0600	Bis(2-ethylhexyl) phthalate*

Note\*: identified for the first time in LHS.

**Table 2**

The physicochemical and pharmacokinetic properties of the potentially effective components in LHS extracts.

Compounds	LogS	LogD	LogP	HIA	F <sub>20%</sub>	F <sub>30%</sub>	Caco-2	PPB	VDss	Fu	CL	T <sub>1/2</sub>
Syringic acid	-1.98	3.98	1.21	0.03	0.01	0.07	-5.14	0.51	0.46	0.39	7.21	0.95
2,3-Dihydroxybenzoic acid	-1.37	1.07	1.58	0.07	0.29	0.97	-5.55	0.71	0.33	0.21	9.14	0.94
4-Methoxysalicylic acid	-2.19	2.92	2.28	0.01	0.01	0.85	-5.10	0.74	0.33	0.21	7.51	0.89
Caffeic acid	-1.12	1.02	1.43	0.01	0.01	0.45	-5.22	0.88	0.37	0.11	10.97	0.93
Ferulic acid	-1.76	2.72	1.80	0.03	0.05	0.58	-4.90	0.90	0.34	0.06	7.48	0.93
Myristicin	-3.25	2.74	2.67	0.00	0.02	0.53	-4.42	0.92	1.23	0.03	14.28	0.69
Syringaldehyde	-2.00	1.05	0.86	0.03	0.00	0.01	-4.66	0.81	0.65	0.16	8.82	0.90
Atractylenolide III	-3.61	3.35	2.90	0.01	0.01	0.01	-4.67	0.72	1.05	0.24	10.72	0.16
Curcolone	-3.98	2.87	2.44	0.03	0.01	0.01	-4.78	0.94	2.47	0.04	13.43	0.35
Dihydrokaempferol	-2.73	0.26	0.85	0.01	0.72	0.10	-5.61	0.83	1.64	0.23	6.52	0.77

Note: LogS (Log of the aqueous solubility); LogD (logP at physiological pH 7.4); LogP (Log of the octanol/water partition coefficient); HIA (Human intestinal absorption); F<sub>20%</sub> (20% bioavailability); F<sub>30%</sub> (30% bioavailability); Caco-2 (Caco-2 permeability); PPB (Plasma protein binding); VDss (Volume distribution); Fu (The fraction unbound in plasmas); CL (Clearance); T<sub>1/2</sub> (Half-life period).

HSD was 0.67-fold lower than in the control group (Fig. 2H). MET and LHS ins counteracted these effects except for glycogen, and the efficacy of LHS extracts was dose-dependent. The HLHS group exhibited the best effect in these parameters, equivalent to MET. Although the glycogen level of flies reared on the LHS extracts diet and control diet did not significantly differ, we noticed a slight reduction for all concentrations.

### 3.3. Metabolomic analysis

#### 3.3.1. The metabolites of flies in different groups were clearly separated in multivariate statistical analysis

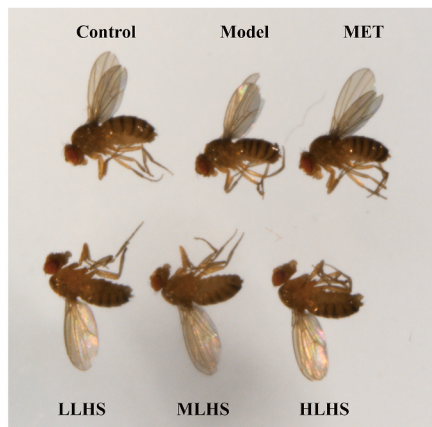
A metabolomic analysis was performed to further verify the effects of LHS extracts on glucolipid metabolism. QC samples were used to validate the precision of the instrument, the repeatability of the method and the stability of the samples. The relative standard deviation (RSD) % of the peak intensities of 10 randomly selected ion peaks were estimated to be 0.69–13.63% (Tables S1–S3), indicating that the method was reliable and the acquired data was high quality. Subsequently, unsupervised PCA and supervised OPLS-DA were performed to evaluate the separation between the three groups. From the scatter plot (Fig. 2A and B), no outlier was found in the PCA analysis. A clear separation between the control group, model group and HLHS group was observed in both positive and negative ion modes, which suggested that the HSD induced significant metabolic change in flies, while the treatment with LHS extracts exhibited a trend of callback. An OPLS-DA model was created to identify significantly differential metabolites between groups and

validated using permutation tests (Fig. 3C–F), resulting in an interpretation rate (R<sub>2</sub>) and prediction ability (Q<sub>2</sub>) of 0.982–0.998 0.992, 0.998, 0.982, 0.996 ( $p < 0.05$ ) and 0.726–0.948 0.948, 0.853, 0.726, 0.753 ( $p < 0.05$ ), respectively (Fig. S12). It demonstrated that the OPLS-DA model was suitable for screening for differential metabolites without overfitting.

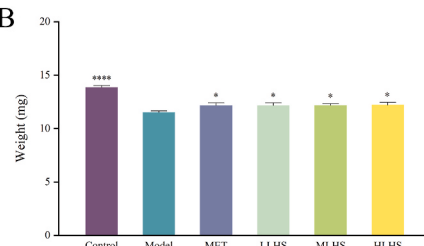
#### 3.3.2. LHS extracts reversed metabolic changes of multiple phospholipids in flies with HSD principally via sphingolipid metabolism

According to the screening condition with VIP  $>1$ ,  $p < 0.05$  and FC  $>2$ , 950 and 473 metabolites were selected as differential metabolites between the control group and model group in positive and negative ion modes, respectively (Fig. 4A). In addition, 291 and 241 metabolites were considered as differential metabolites between the model group and HLHS group in positive and negative ion modes, respectively. Thereinto, treatment with LHS extracts observably contributed to 23 and 57 metabolites in positive and negative ion modes, which were considered the effect biomarkers of LHS extracts. Furthermore, 21 effect biomarkers were identified, including phospholipids, amino acids, purines, and indoles (Table S4). Specifically, the levels of N-alpha-acetyl-L-citrulline, 3-indolebutyric acid, 2-oxoarginine, N-eicosapentaenoyl cysteine, N-eicosapentaenoyl methionine, octanoylcarnitine, sphinganine 1-phosphate, PS(PGF1alpha/22:1(13Z)), dihydro-2,4,6-tris(2-methylpropyl)-4H-1,3-dithiazine, indole-5,6-quinone, 5-pyridoxolactone, (2R)-2-hydroxy-2-methylbutanenitrile and oxidised glutathione that were significantly higher in flies with HSD were reduced by LHS extracts. The levels

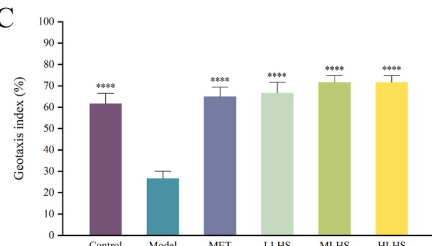
A



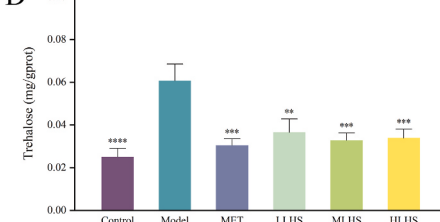
B



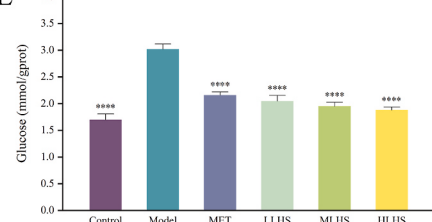
C



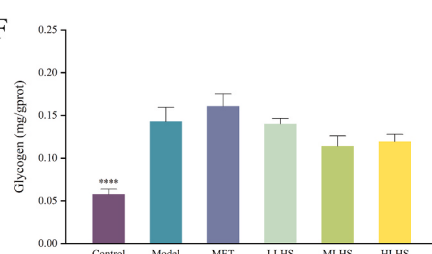
D



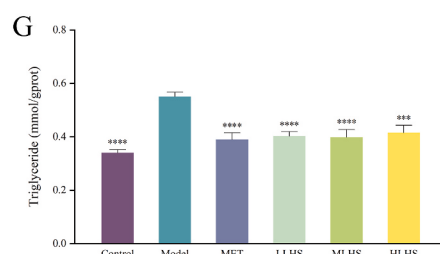
E



F



G



H

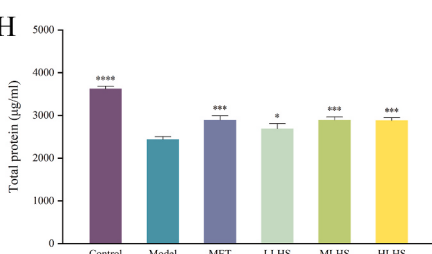


**Fig. 2.** The regulation of the disorder of glucolipid metabolism induced by the HSD in flies using LHS extracts. The morphology of flies in different groups (A). Effect of LHS on body weight (B), geotaxis index (C), trehalose level (D), glucose level (E), glycogen level (F), triglyceride level (G) and total protein level (H) of flies exposed to the HSD. Data are presented as mean  $\pm$  SEM ( $n = 6$ ) by one-way ANOVA followed by LSD test. \* $p < 0.05$ , \*\* $p < 0.01$ , \*\*\* $p < 0.001$ , \*\*\*\* $p < 0.0001$ , compared to the model group.

of 4-acetamido-2-aminobutanoic acid, PA(20:0/16:1(9Z)), DG(i-20:0/PJG2:0:0), vanillin 4-sulfate, lysoPC(6:0/0:0), xanthine, uridine and ectoine were upregulated, most of which exhibited no significant difference compared to the control group (Fig. 4B). In particular, LHS extracts further reversed the levels of oxidised glutathione and 5-pyridoxolactone, demonstrating that they played essential roles in the treatment with LHS extracts. The relative content of 21 identified metabolites in each sample was visualised by a heat map, showing that these metabolites were clearly separated between groups and were supposed to be the effect biomarkers of LHS extracts (Fig. 4C). To reveal the key pathways changed during the treatment with LHS extracts, the effect biomarkers were further analysed by Massdatabase, a R-language package. The chosen metabolites were mapped to KEGG metabolic pathways of *Drosophila melanogaster* for over-representation and pathway analyses. Glycine, serine and threonine metabolism, caffeine metabolism, arginine biosynthesis, sphingolipid metabolism, vitamin B6 metabolism, glutathione metabolism, etc., were closely related to the changes in metabolic levels (Fig. 4D). Notably, sphingolipid metabolism played an essential role in regulating other metabolic pathways. In addition, most of the effect biomarkers were also relevant to sphingolipids. Therefore, LHS extracts may be able to alleviate glucolipid metabolism disorders owing to their involvement in sphingolipid metabolism.

### 3.4. RNA sequencing

#### 3.4.1. LHS extracts extensively regulated gene expression in the sphingolipid signalling pathway

Transcriptomic analysis using RNA sequencing was performed to reveal the underlying mechanisms of LHS extracts in regulating the disorder of glucolipid metabolism. A total of 16,836 genes were identified in flies, almost half exhibiting a significant change compared to

the control group due to the HSD. Whereas LHS extracts significantly shifted the transcriptomic profile in HSD flies (Fig. S13A). As shown in Fig. S13B, 1145 genes were considered SDEGs in the model group compared to the control group, with 1062 upregulated and 83 downregulated. Based on KEGG enrichment analysis, these SDEGs were significantly enriched in insulin secretion (Fig. S13D). In addition, several receptors and channel activities were closely related to the changes in transcriptomic profile, according to GO-molecular function (GOMF) analysis (Fig. S13E). Furthermore, 241 SDEGs were identified between the model group and the HLHS group, with 45 upregulated and 196 downregulated (Fig. S13C). KEGG enrichment analysis demonstrated that these SDEGs were potentially involved in the lysosome, apoptosis, sphingolipid signalling pathway, etc. (Fig. 5A) Correspondingly, GOMF analysis suggested that LHS extracts significantly regulated multiple phospholipase activities related to sphingolipids, including phospholipase activity, phospholipase A1 activity, acid sphingomyelin phosphodiesterase activity and sphingomyelin phosphodiesterase activity (Fig. 5B). Combined with the KEGG enrichment analysis result, the sphingolipid signalling pathway was supposed to be the key transcriptomic enrichment pathway. As shown in Fig. 5D, DEGs enriched in the sphingolipid signalling pathway were further categorised into two subsets depending on their regulative effects, most of which were upregulated. Consistent with the cluster heatmap, GSEA analysis indicated the upregulation of genes involved in the sphingolipid signalling pathway (KEGG entry: map04071) (Fig. 5C). To this end, we further evaluated the changes in expression levels of upregulated DEGs induced by LHS extracts when compared to the control group (Fig. 5E). The HSD resulted in decreased expression levels of these genes. In contrast, LHS extracts exhibited a reversible effect on these genes, which showed no significant difference compared to the control group. Interestingly, a majority of upregulated DEGs were concerned with the PI3K-Akt signalling pathway, such as *Pi3K21B*, *Pdk1*, *Akt1*, *Ras85D*, *Mtl* and *Galphai*,

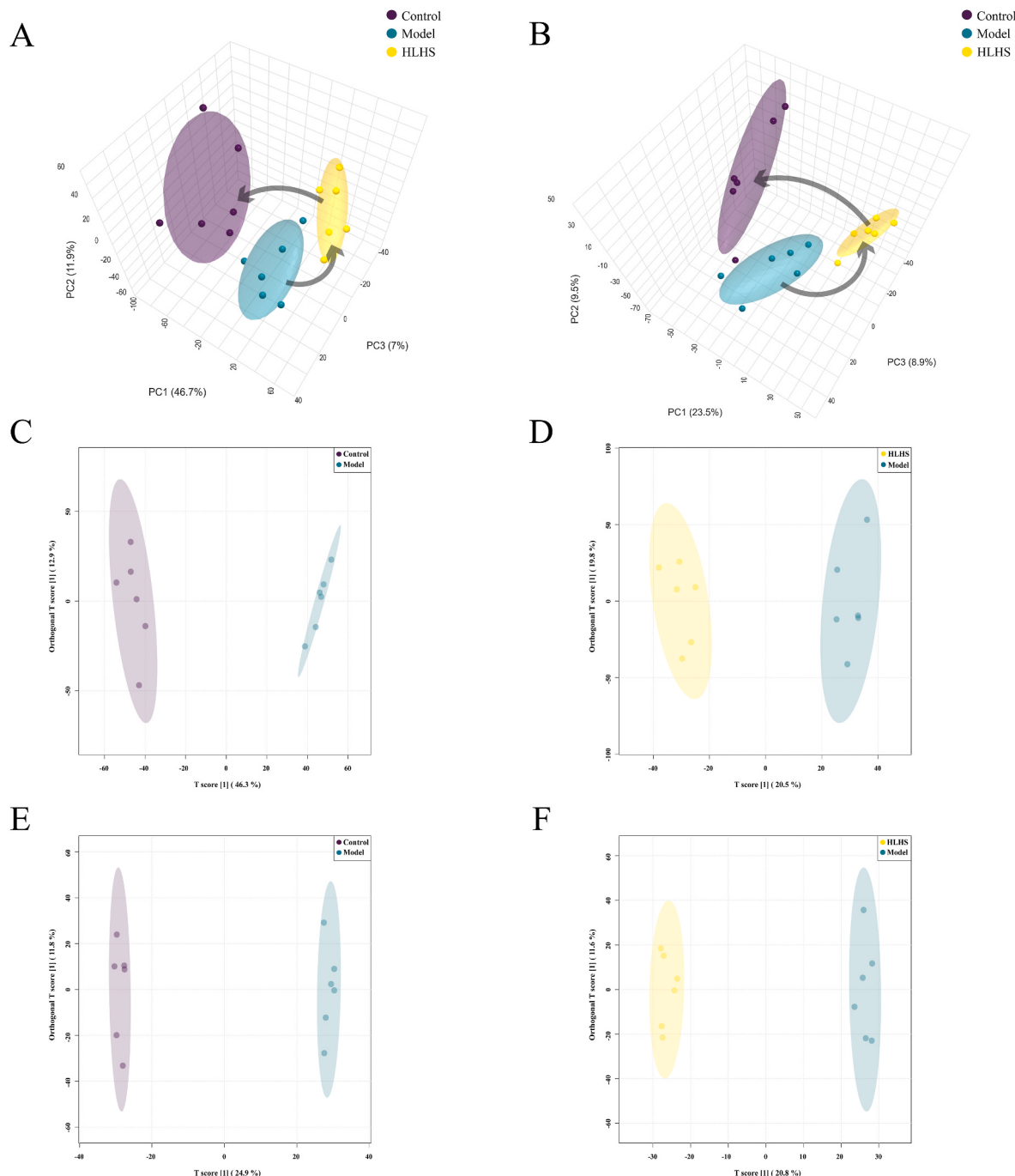


**Fig. 3.** Multivariate statistical analysis of non-targeted metabolomics. PCA scoring plots for metabolites of flies in positive mode (A) and negative mode (B). OPLS-DA scoring plots for metabolites of flies from the control and model group in positive mode (C) and negative mode (E). OPLS-DA scoring plots for metabolites of flies from the model and HLHS group in positive mode (D) and negative mode (F).

whereas the expression of most DEGs relevant to lysosomes was significantly reduced. All of the SDEGs enriched in the sphingolipid signalling pathway were responsible for the inhibition of apoptosis mediated by lysosomes, including *CG31661*, *CG31926*, *CG6508* and *CG31928*. These findings corresponded to the cross-regulation mediated by the S1P axis. Therefore, we deduced that the extensive regulation of the expression of genes involved in the sphingolipid signalling pathway by LHS extracts may subsequently modulate the PI3K-Akt signalling pathway and lysosome-mediated apoptosis.

#### 3.4.2. LHS extracts activated the PI3K-Akt signalling pathway and inhibited lysosome-mediated apoptosis potentially via the sphingolipid signalling pathway

Since the PI3K-Akt signalling pathway and lysosomes seized the principal position in the downstream pathways of sphingolipid signalling, the results described above led us to explore the involvement of these pathways in the regulation of LHS extracts. As shown in Fig. 6A, the upstream genes of the PI3K-Akt signalling pathway were extensively upregulated, such as *hop*, *Fak*, *Pi3K21B*, *Pdk1*, *Akt1*, *Ras85D*, *Mtl* and *Cdc37*, consistent with the upregulated DEGs enriched in the sphingolipid signalling pathway. As a result, critical genes responsible for glycogen and protein synthesis, including *GlyS*, *eIF4EHP* and *eIF4E1*,

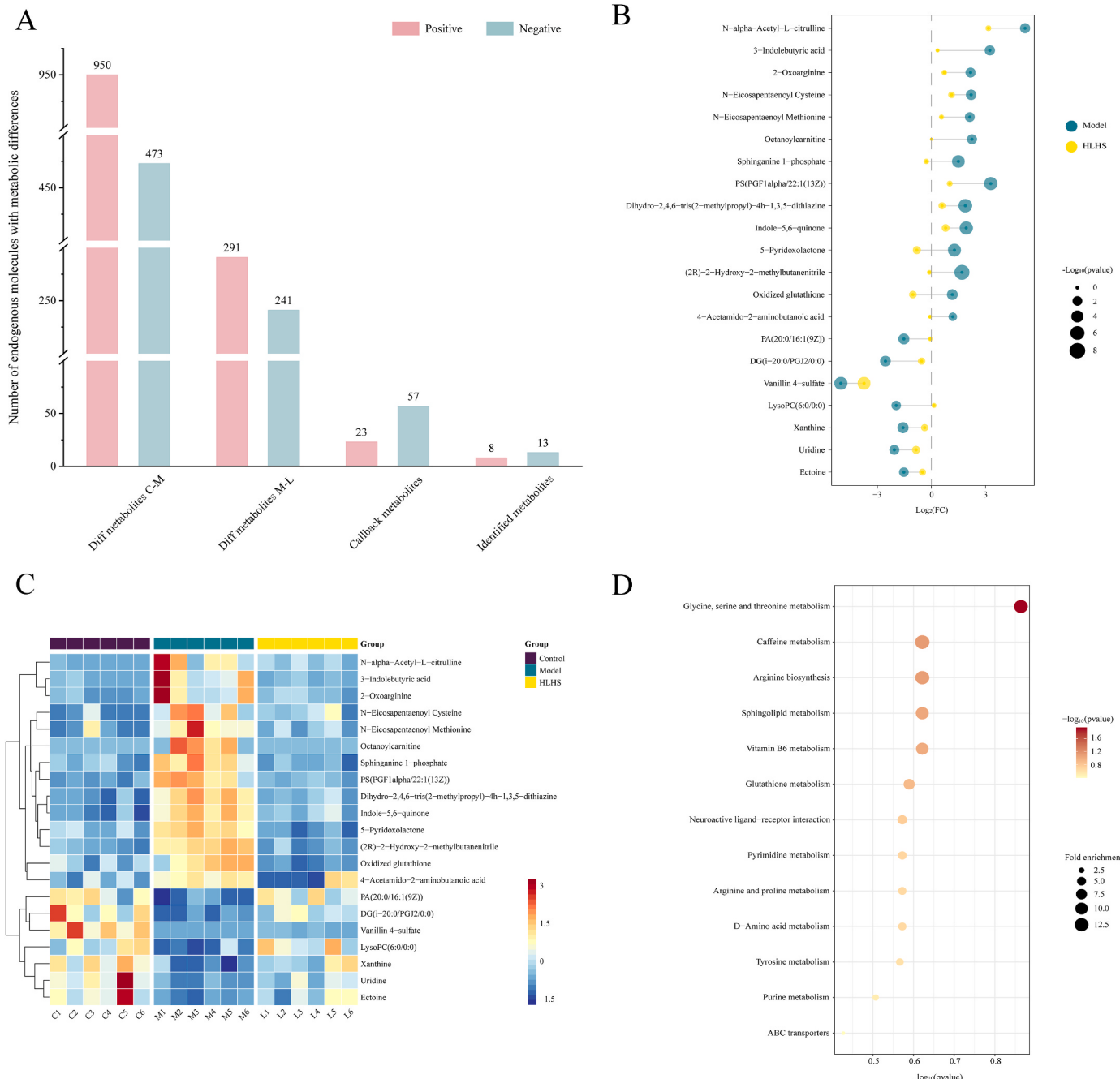


**Fig. 4.** The regulation of the disorder of metabolites in flies using LHS extracts via non-targeted metabolomics. (A) Screening process of the effect biomarkers of LHS extracts regulating the disorder of glucolipid metabolism. (B) Changes of the effect biomarkers of LHS extracts in the model group and HLHS group, when compared to the control group. (C) Changes in relative content of the effect biomarkers of LHS extracts. (D) Metabolic pathway enrichment analysis of the effect biomarkers of LHS extracts based on KEGG database.

were significantly upregulated by LHS extracts. In contrast, essential genes implicated in gluconeogenesis, such as *Pepck1*, *Pepck2* and *CG45087*, were downregulated. In conjunction with the GSEA analysis (KEGG entry: map04151) (Fig. 6B), these results demonstrated that LHS extracts positively regulated the PI3K-Akt signalling pathway. We, therefore, investigated whether LHS extracts could reverse the negative regulation of these genes induced by the HSD. As expected, most of the positively regulated DEGs by LHS extracts showed no significant difference compared to the control group (Fig. 6C), suggesting that LHS extracts activate the PI3K-Akt signalling pathway probably via the sphingolipid signalling pathway.

Next, we sought to confirm whether lysosomes were impacted in the

treatment with LHS extracts. DEGs related to lysosomes were plotted in Fig. 6D as a heatmap, indicating that LHS extracts significantly shifted the transcriptomic profile involved in the lysosome. Moreover, 14 lysosomal acid hydrolases, as well as 8 lysosomal membrane proteins, were suppressed by transcriptionally modulating gene expression, such as cathepsins, beta-galactosidase, glucocerebrosidase 1b, N-sulfoglucosamine sulfohydrolase, lipase 4, deoxyribonuclease II, battenin, etc. Consistently, GSEA analysis (KEGG entry: map04142) revealed that the expression of genes involved in the lysosome was significantly decreased by LHS extracts (Fig. 6E). Specifically, *CG31661*, *CG31926*, *CG6508* and *CG31928*, genes encoding cathepsins, were identified as SDEGs, which played an essential role in lysosome-mediated apoptosis. These findings

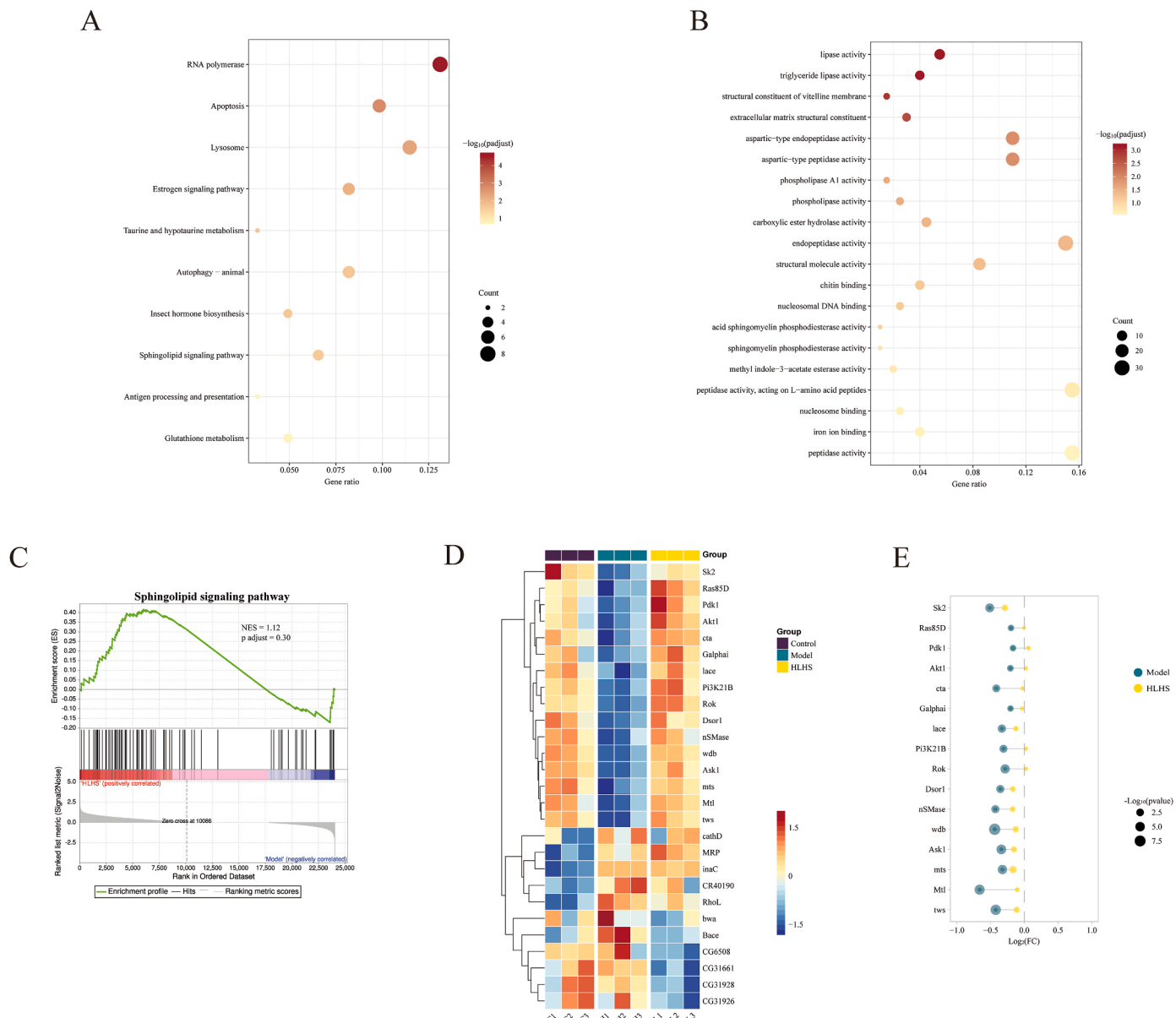


**Fig. 5.** The regulation of the transcriptome of T2DM flies using LHS extracts. (A) KEGG pathway enrichment analysis based on SDEGs in the HLHS group vs. the model group. (B) GOMF pathway enrichment analysis based on SDEGs in the HLHS group vs. the model group. (C) GSEA plot for KEGG entry: Sphingolipid signalling pathway based on all genes in the HLHS group vs. the model group. (D) Changes in relative expressions of DEGs involved in the sphingolipid signalling pathway in different groups. (E) Changes in relative expressions of upregulated significant genes involved in the sphingolipid signalling pathway in the model group and HLHS group, when compared to the control group.

were also in accordance with the KEGG enrichment analysis. Together, these data suggest that LHS extracts inhibit lysosome-mediated apoptosis potentially via the sphingolipid signalling pathway.

#### 3.4.3. LHS extracts alleviated the disorder of glucolipid metabolism by modulating the S1P axis

As the directly upstream pathway, sphingolipid metabolism greatly contributed to controlling the sphingolipid signalling pathway. According to the previous analysis, sphingolipid metabolism was supposed to be the key metabolic enrichment pathway based on non-targeted metabolomics. Thus, DEGs relevant to this pathway were further investigated to reveal the potential regulation by LHS extracts. As shown in Fig. 6G, a total of 12 genes involved in sphingolipid metabolism were identified, and half of the genes were downregulated by LHS extracts, while half were upregulated. All of these genes are located on the S1P axis, suggesting that LHS targeted the S1P axis rather than extensively

regulated sphingolipid metabolism. GSEA analysis (KEGG entry: map00600) further demonstrated that upregulated genes were enriched in the HLHS group, implying that LHS extracts were more potent in promoting sphingolipid metabolism. Integrative analysis of transcriptomic and metabolomic data strongly suggested that the clearance of dhS1P by LHS extracts was attributed to the increased expression of *wun2* (Fig. 6I). However, *Sk2*, a gene responsible for producing dhS1P, was paradoxically upregulated, accompanied with downregulation of *laza*, a gene catalysing the transformation of dhS1P into dhSph. These results indicated that LHS extracts modulated the S1P axis in a complicated way, which was comprehensively regulated to suppress the accumulation of sphingolipids instead of simply activating them. Consistent with this, the expression of DEGs located on the S1P axis was reversed by LHS extracts and exhibited normal levels (Fig. 6H). Although S1P and Cer were not identified based on non-targeted metabolomics due to technical limitations, the genes responsible for

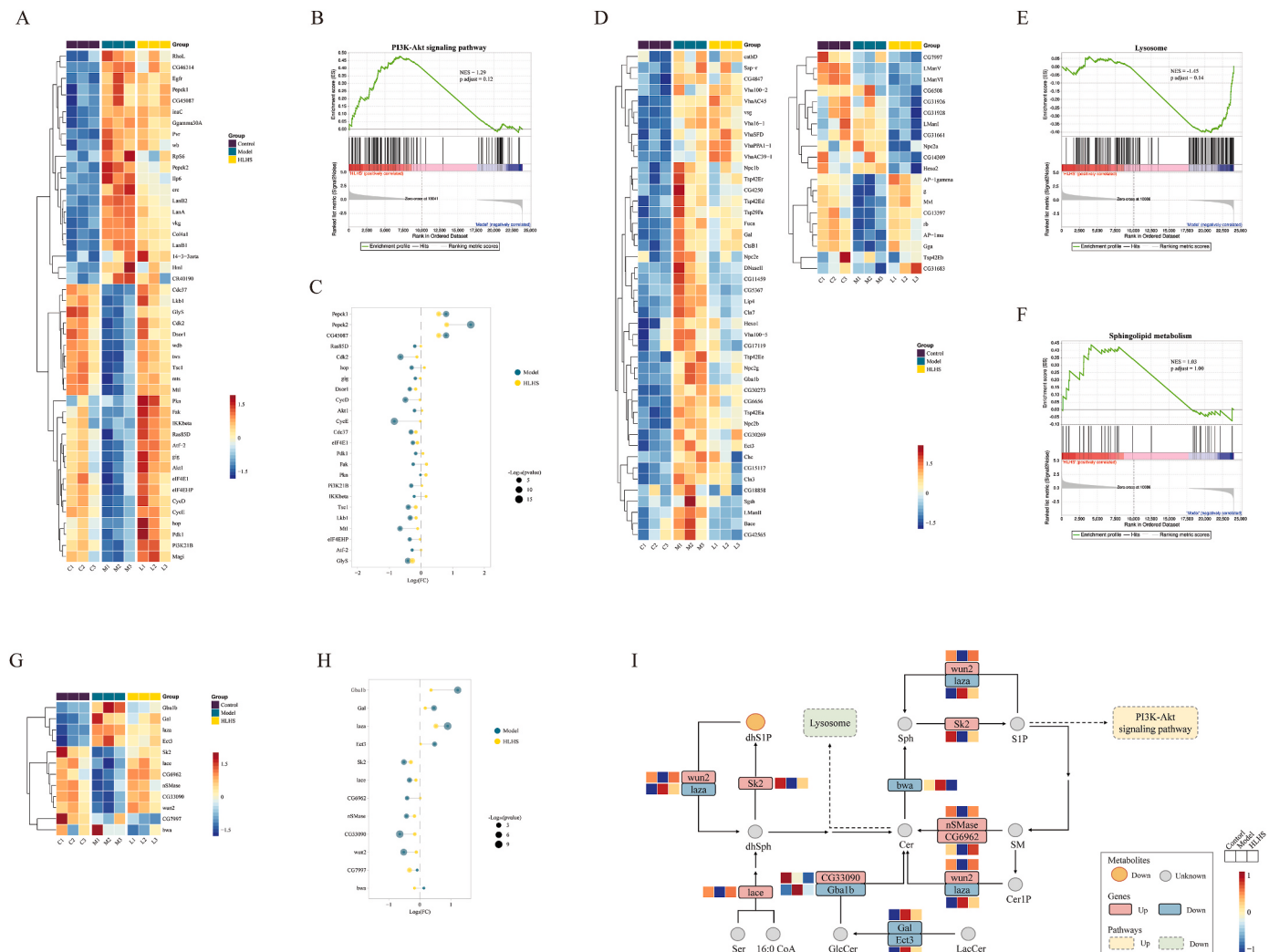


**Fig. 6.** Effects of LHS extracts on the PI3K-Akt signalling pathway, lysosomes and sphingolipid metabolism. (A) Changes in relative expressions of DEGs involved in the PI3K-Akt signalling pathway in different groups. (B) GSEA plot for KEGG entry: PI3K-Akt signalling pathway based on all genes in the HLHS group vs. the model group. (C) Changes in relative expressions of positively regulated DEGs involved in the PI3K-Akt signalling pathway in the model group and HLHS group, when compared to the control group. (D) Changes in relative expressions of DEGs involved in lysosomes in different groups. (E) GSEA plot for KEGG entry: Lysosome based on all genes in the HLHS group vs. the model group. (F) GSEA plot for KEGG entry: Sphingolipid metabolism based on all genes in the HLHS group vs. the model group. (G) Changes in relative expressions of DEGs involved in sphingolipid metabolism in different groups. (H) Changes in relative expressions of DEGs involved in sphingolipid metabolism in the model group and HLHS group, when compared to the control group. (I) Changes in sphingolipid metabolism in the HLHS group vs. the model group. The orange and gray dots represented increased and unknown metabolites after LHS extracts treatment, respectively. The red and blue squares represented upregulated and downregulated genes upon LHS extracts challenges, respectively. The foursquares represented relative expressions of the nearby genes in the control group, model group and HLHS group from left to right, respectively. (For interpretation of the references to colour in this figure legend, the reader is referred to the Web version of this article.)

the production and transformation of S1P and Cer were dramatically changed after LHS extracts treatment (Fig. 6I). Furthermore, S1P and Cer are a major part of the S1P axis and have been well-characterised as the master regulators of the PI3K-Akt signalling pathway and lysosomes, respectively (Johnson and Stolzing, 2019; Takuwa et al., 2012). Specifically, the effects of S1P and Cer were embodied in the positive cross-regulation mediated by the S1P axis. Taken together, we concluded that LHS extracts modulated the S1P axis, thereby activating the PI3K-Akt signalling pathway and inhibiting lysosome-mediated apoptosis via the sphingolipid signalling pathway.

#### 3.4.4. TFs were potential targets of LHS extracts

The above findings demonstrated that LHS extracts modulated the expression profile of S1P axis-related genes on a large scale, implying that upstream TFs, instead of single enzymes, may be the primary molecular targets of LHS extracts. Thus, based on DEGs between the model

group and the HLHS group enriched in sphingolipid metabolism, JASPAR was applied to predict the involved TFs. As shown in Fig. 7A, according to the condition of  $p$  adjust  $<0.0001$ , Cor  $p$  adjust  $<0.05$ , DNA binding domain (DBD)  $>50\%$  and count  $\geq 1$ , 19 TFs were considered as the potential targets of LHS extracts. Due to a majority of the protein structures of 19 TFs derived from *Drosophila melanogaster* being unclear, as well as the lack of antibodies, the follow-up work would be performed on HepG2 cells to verify these results. To this end, we focused on the eight TFs orthologous to human proteins, including ecdysone receptor (EcR, encoded by EcR, homologous protein of NR1H2), protein ultraspire (USP, encoded by usp, homologous protein of RXRA), heat shock factor protein (HSF, encoded by Hsf, homologous protein of HSF1), segmentation protein paired (PRD, encoded by prd, homologous protein of PAX3), protein scalloped (SCAL, encoded by sd, homologous protein of TEAD3), ecdysone-induced protein 75B, isoform A (E75BA, encoded by Eip75B, homologous protein of PPARA), forkhead domain

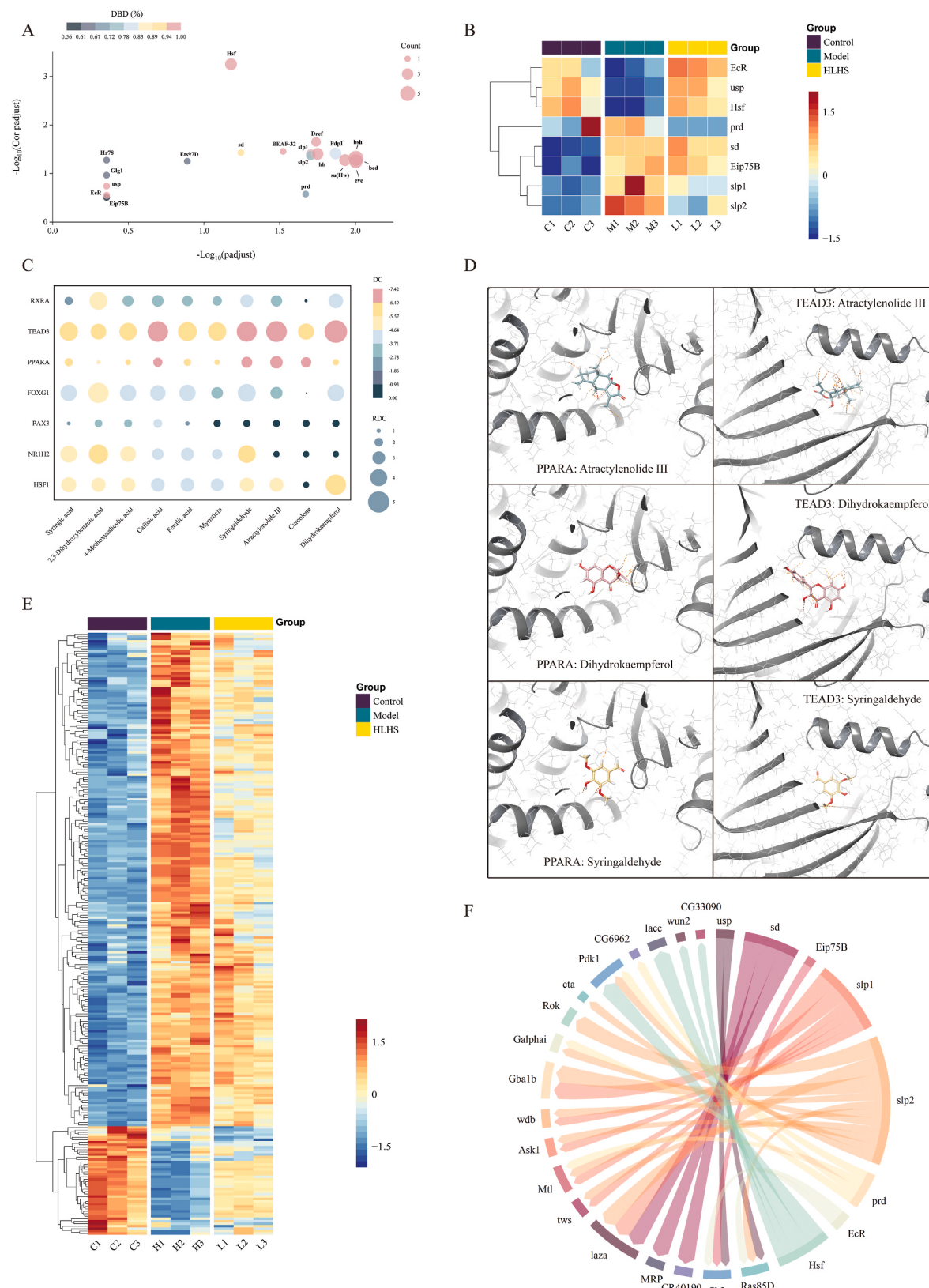


**Fig. 7.** Regulative effects of LHS extracts on TFs involved in sphingolipid metabolism. (A) TFs analysis plot based on the DEGs enriched in sphingolipid metabolism. (B) The expression profile of predicted TFs involved in the regulation of sphingolipid metabolism. (C) Molecular docking results of the potentially effective components binding to TFs. DC and RDC indicating the potential binding affinity were calculated as instructed in the method. (D) The representative images for the binding mode of atractylenolide III (blue), dihydrokaempferol (pink) and syringaldehyde (yellow) with the crystal structure of PPARA (PDB ID: 6KAX, grey) and TEAD3 (PDB ID: 7CNL, grey). (E) The expression profile of *sd* target genes with differential expression between the model group and HLHS group. (F) Regulatory relationships of TFs and their target genes involved in sphingolipid metabolism and the sphingolipid signalling pathway. (For interpretation of the references to colour in this figure legend, the reader is referred to the Web version of this article.)

transcription factor *slp1* (SLP1, encoded by *slp1*, homologous proteins of FOXG1) and forkhead domain transcription factor *slp2* (SLP2, encoded by *slp2*, homologous proteins of FOXG1). The expression patterns of these TFs upon LHS extracts challenge were further shown in Fig. 7B. All of them exhibited significant difference between the control group and model group, while LHS extracts reversed the changes of transcriptomic profile except for *sd* and *Eip75B*. The molecular simulation was then employed to further explore the potential binding of the potentially effective components with these TFs (Fig. 7C). In Fig. 7C, the colour of each dot represented the DC of compounds, and the size of dots indicated the binding affinity of the potentially effective components when compared to the original ligands in the protein crystal structure complex. Therein, all of the 10 compounds were observed as the potential inhibitors of TEAD3, a transcriptional enhancer factor, by blocking the palmitoyl-CoA binding site when compared to the original ligand CH<sub>3</sub>(CH<sub>2</sub>)<sub>12</sub>CONHOH (Tang et al., 2021). Consistently, *laza*, *MPR* and *CR40190*, the target genes of *sd*, were downregulated by LHS extracts. The molecular docking results further showed the plausible binding mode of TEAD3 with atractylenolide III, dihydrokaempferol and syringaldehyde, which owned the top 3 RDC (Fig. 7D). Furthermore, by investigating the expression patterns of *sd* target genes, we found that more than three-quarters of these target genes were downregulated by LHS extracts, and only less than 15% were upregulated (Fig. 7E). These results strongly suggested that *sd* was one of the most potential targets of LHS extracts. Moreover, PPARA might also be activated by all of the 10 compounds with the lower DC when compared to the original activator, palmitic acid (Kamata et al., 2020). Corresponding to the result, *Sk2*, the target gene of *Eip75B*, was significantly upregulated by LHS extracts. Interestingly, the top 3 RDC also belonged to atractylenolide III, dihydrokaempferol and syringaldehyde, with which the plausible binding mode of PPARA was shown in Fig. 7D. These results indicated that *Eip75B* might contribute to the regulative effect of LHS extracts. It is noteworthy that the rest of the TFs could be potentially activated or repressed by at least five compounds according to RDC, implying that the modulation of LHS extracts may be relevant to multiple targets and components instead of a single. We thereby investigated the regulatory relationships of the TFs and their target DEGs involved in sphingolipid metabolism and the sphingolipid signalling pathway. As shown in Fig. 7F, these TFs modulated the expression of the S1P axis-related genes on a large scale. We, therefore, proposed that LHS extracts regulated the S1P axis via activating TF networks, including *sd*, *Eip75B*, *usp*, *slp1*, *slp2*, *prd*, *EcR* and *Hsf*. However, further experimental evidence is still required for validation.

#### 4. Discussion

Here, we demonstrated that LHS extracts alleviated the disorder of glucolipid metabolism in HSD-induced T2DM fruit flies, as indicated by decreased trehalose, glucose and triglyceride levels and increased total protein levels. Moreover, we identified 76 chemical components in LHS extracts based on UPLC-Q Exactive-Orbitrap-MS, including 65 chemical components for the first time. Furthermore, by applying integrative metabolic and transcriptomic analysis, we systematically evaluated the specific effects of LHS extracts on sphingolipid metabolism and the expression profile of genes implicated in the sphingolipid signalling pathway. Importantly, we proposed that LHS extracts alleviated the disorder of glucolipid metabolism via the positive cross-regulation mediated by the S1P axis in T2DM fruit fly and that upstream TFs were the potential targets.

##### 4.1. Comprehensive characterisation of small molecules in LHS extracts

Previously, only a small number of compounds in LHS have been identified, including polyacetylenes, phenylpropanoids and their glycosides (Kim et al., 2017; Tan et al., 1998; Guang et al., 1997); therefore, the substantial basis of LHS remains undefined. Hence, it would be of

great interest to comprehensively characterise the small molecules based on UPLC-Q Exactive-Orbitrap-MS. In addition to polyacetylenes, phenylpropanoids and their glycosides, our data showed that flavonoids and organic acids were prominent in the chemical components, which redefined the chemical profile of LHS. This part of the work laid a firm foundation for researching the effective substances of LHS.

##### 4.2. Regulation of the disorder of glucolipid metabolism in T2DM fruit fly by LHS extracts

With abundant natural resources, LHS is merely used in folk medicine in southern China, in large part due to the lack of pharmacodynamics research. Under the guidance of TCM, we proposed that LHS was a potential candidate for anti-T2DM drugs. Consequently, HSD-induced T2DM flies were applied to evaluate the effect of LHS. The decrease in body weight and climbing ability were considered phenotypic responses of T2DM in flies (Baenas and Wagner, 2022; Ecker et al., 2017), which was observed in our study. Notably, a high dose of LHS extracts demonstrated efficacy over MET in these evaluation indexes, suggesting that LHS extracts could preferably improve the physiological state of the body. As in humans, flies' main circulating energy sources are sugars, with trehalose (the predominant one) and glucose found in the hemolymph (Galikova and Klepsat, 2018). Furthermore, excess dietary sugar can be transferred to tissues to be stored as glycogen or triglycerides in fat bodies (Sang et al., 2021). Both trehalose and glucose have been reported to increase with HSD exposure in flies, as well as triglycerides and glycogen (Ecker et al., 2017; Sang et al., 2021). On the contrary, the reduction of total protein has been investigated in T2DM flies (Kayode et al., 2021). Correspondingly, our results showed the same changes in the model group, while significant reversions except glycogen were detectable in flies fed with LHS extracts and MET. According to a previous study, the level of glycogen was not affected by MET and tested drugs in flies, which may attribute to the different ways of sugar clearance in flies (Cao et al., 2022). Considering the satisfactory effects on the rest of the assays, we concluded that LHS regulated the disorder of glucolipid metabolism in T2DM flies. Our work provided experimental evidence supporting LHS as a candidate for anti-T2DM drugs and further broadened the development space for LHS.

##### 4.3. The positive cross-regulation mediated by the S1P axis in LHS extracts treating with T2DM fruit fly

Sphingolipids, including ceramides, sphingomyelins, and cerebrosides, contribute to physiological and pathological processes in T2DM patients and animal models (Lai et al., 2016). For instance, ceramides, glucosylceramides (GluCer) and the dhS1P/dhSph ratio are elevated in the plasma of human T2DM patients (Chen et al., 2021; Haus et al., 2009; Serlie et al., 2007). Specifically, multiple studies have demonstrated that ceramides promoted the dysfunction and apoptosis of pancreatic  $\beta$  islet cells in vitro and in vivo and that inhibition of ceramide synthesis improves insulin sensitivity (Aerts et al., 2011; Chavez et al., 2003; Chavez and Summers, 2012), whereas S1P are exactly converse (He et al., 2021). Cer is converted to Sph, and Sph is phosphorylated to form S1P. These metabolites constitute the S1P axis, which is strictly regulated in time and space. The metabolic pathway of sphingolipids appears to be conserved between *Drosophila melanogaster* and mammals (Yang et al., 2010). In the current study, dhS1P was remarkably decreased in T2DM flies treated with LHS extracts, corresponding to the biomarker of T2DM according to the previous study (Chen et al., 2021). Meanwhile, genes located on the S1P axis were significantly modulated by LHS extracts. Notably, most of these genes were directly associated with the synthesis and decomposition of S1P and Cer, implying that the S1P axis, instead of sphingolipid metabolism, was the target of LHS extracts. Therein, transcription of *Sk2* played an essential role in the transformation from Sph to S1P and was perceived to be the master gene to suppress the hepatic glucose production and IR

in mice, which was observably enhanced by LHS extracts (Aji et al., 2020). Paradoxically, the genes encoding several enzymes that jointly controlled the transformation of S1P and Cer exhibited the opposite effects to each other in the regulation of LHS extracts. Specifically, *wun2* and *CG33090*, the genes responsible for the conversion of S1P and Cer, respectively, were upregulated, while *laza* and *Gba1b*, with similar biological functions, were downregulated. Together, these results indicated that LHS extracts regulated the S1P axis in a complicated way, which was to eliminate the accumulation of sphingolipids and maintain the homeostasis of the S1P axis. Furthermore, the cross-regulation mediated by the S1P axis was observed in the sphingolipid signalling pathway based on transcriptomic analysis. As the direct target of Cer, cathepsins are engaged in key events of cellular apoptosis and lysosomal IL-1 $\beta$  release, which is implicated in the pathogenesis of T2DM (Marekowska et al., 2023; Tseng et al., 2017). By transcriptionally modulating gene expression of cathepsins as well as the genes involved in lysosome-mediated apoptosis, LHS extracts may improve the adverse effects of T2DM. In mammals, S1P is both an extracellular and intracellular signalling molecule and has been shown to bind five different G protein-coupled receptors (Pantoja et al., 2013). There do not appear to be S1P G protein-coupled receptors in flies, but the guanine nucleotide-binding G protein alpha i subunit (GNAI) does exist in flies. The expression of *Galphai* (encoding GNAI) and the downstream gene, *Pi3K21B* (encoding a homologous protein of PI3K), as well as PI3K-Akt signalling pathway, was promoted by LHS extracts, which was consistent with S1P suppressing IR through the GNAI-mediated PI3K-Akt signalling pathway (He et al., 2021; Takuwa et al., 2012). Of note, downstream genes directly involved in the regulation of glucose metabolism were modulated, including *GlyS* (genes implicated in glycogen), *eIF4EHP*, *eIF4E1* (genes implicated in protein synthesis), *Pepck1*, *Pepck2* and *CG45087* (genes implicated in gluconeogenesis). These data supported our idea that the homeostasis of the S1P axis was the basis of the positive cross-regulation mediated by the S1P axis in T2DM treatment with LHS extracts. Our study revealed potential mechanisms of the S1P axis in LHS treating T2DM fruit fly and provided new ideas for targeted therapeutic drug development.

#### 4.4. TF networks as the basis of LHS efficacy in T2DM fruit fly

TFs represent the point of convergence of multiple signalling pathways within eukaryotic cells and extensively modulate gene expression by influencing RNA polymerase II activity in a gene-specific manner (Papavassiliou and Papavassiliou, 2016). In accordance with transcriptomic analysis, multiple genes on the S1P axis were paradoxically regulated by LHS extracts, indicating that upstream TFs were involved. TF orthologs between humans and *Drosophila melanogaster* often display virtually identical sequence specificity, and the physiological roles of TFs are also often conserved (Lambert et al., 2018). Therefore, considering the unknown protein structures of *Drosophila melanogaster* TFs and the follow-up work, human proteins orthologous to *Drosophila melanogaster* TFs were applied for molecular simulation. Among these TFs, TEAD3 was the most potential target of LHS extracts. Though there is no evidence shown that TEAD3 contributes to the pathogenesis of T2DM, the most recent study has revealed that the inhibition of the Hippo signal pathway could alleviate high glucose-induced pyroptosis, of which TEAD3 was a master regulator (Hong et al., 2021). By molecular docking, all of the effective components were observed as potential inhibitors of TEAD3. In flies, the expression profile of the target genes of *sd*, the gene encoding a homologous protein of TEAD3, was correspondingly suppressed, especially *laza*, which was responsible for the conversion of S1P and Cer. PPARA was engaged in key events of lipid metabolism and consequently indicated for the treatment of hypertriglyceridemia in T2DM (Nanjan et al., 2018). As predicted by molecular docking, the effective components in LHS extracts might also directly bind to PPARA and at least partly act as PPARA agonists. Further transcriptomic analysis suggested that the target genes of *Eip75B*, the gene encoding a

homologous protein of TEAD3, were partly upregulated, including the core gene on the S1P axis, *Sk2*. Thus, these results demonstrated that LHS extracts modulated the S1P axis via a complex interaction between the effective components-mediated regulation of TFs in T2DM fruit fly. Our work encouraged systemic exploration of the relationships among TF networks, the S1P axis and T2DM treatment.

#### 4.5. Limitations of the study

We acknowledge some limitations of this study. First, the underlying mechanisms of the cross-regulation mediated by the S1P axis in LHS extracts alleviating the disorder of glucolipid metabolism still need to be addressed in further studies. Second, more experimental evidence is urgently required to elucidate the complex interaction between the effective components-mediated regulation of TFs. Third, only the fly model was acquired for this study, and further pharmacodynamics and metabolomics studies with human cells would validate our evidence. Fourth, the chemical analysis of LHS extracts in this study was limited to the small molecules, whereas polysaccharides were unacknowledged and supposed to be investigated in the follow-up work.

### 5. Conclusions

The current study systematically demonstrated that LHS extracts significantly ameliorated the disorder of glucolipid metabolism in the HSD-induced T2DM fruit fly model. In accordance with UPLC-Q Exactive-Orbitrap-MS, we identified 76 chemical components in LHS extracts, including 65 for the first time, and redefined the chemical profile of LHS with flavonoids and organic acids being prominent in the chemical components. Integrative metabolomic and transcriptomic analysis revealed that LHS extracts eliminated the accumulation of sphingolipids and subsequently stimulated the positive cross-regulation mediated by the S1P axis, resulting in the activation of PI3K-Akt signalling pathway and inhibition of lysosome-mediated apoptosis. Bioinformatic analysis revealed that the upstream TFs, TEAD3 and PPARA, were the potential targets of atractylenolide III, dihydrokaempferol and syringaldehyde, the potentially effective components of LHS extracts. Our study not only sheds novel light on the complicated mechanisms underlying the anti-T2DM activities of herbal medicine LHS but also provides critical evidence inspiring the discovery and development of innovative therapeutic agents based on the cross-regulation mediated by the S1P axis for treating T2DM and related complications.

#### CRediT authorship contribution statement

Gengyuan Yu: Investigation, Methodology, Visualization, Data curation, Formal Analysis, Writing – original draft. Mo Sun: Visualization, Formal Analysis, Writing – review and editing. Tonghua Zhang: Investigation, Methodology. Haoran Xu: Methodology, Project administration. Jiaqi Wang: Methodology, Formal Analysis. Wanting Ye: Investigation, Formal Analysis. Peng Wang: Supervision. Shiyun Zhang: Supervision. Chenning Zhang: Conceptualization, Funding acquisition, Writing – review and editing. Yikun Sun: Conceptualization, Funding acquisition, Resources. All authors contributed to the review of the manuscript and approved the final version for publication.

#### Funding

This work was supported by 2022 Medical and Health Science and Technology Plan of Xiangyang City, Hubei Province (No. 2022YL30A) and Natural Science Foundation of Hubei Province (No. 2022CFB867).

#### Declaration of competing interest

The authors declare that they have no known competing financial interests or personal relationships that could have appeared to influence

the work reported in this paper.

## Data availability

Data will be made available on request.

## Appendix A. Supplementary data

Supplementary data to this article can be found online at <https://doi.org/10.1016/j.jep.2023.117248>.

## References

- Aerts, J.M., Boot, R.G., van Eijk, M., Groener, J., Bijl, N., Lombardo, E., Bietrix, F.M., Dekker, N., Groen, A.K., Ottenhoff, R., van Roomen, C., Aten, J., Serlie, M., Langeveld, M., Wennekes, T., Overkleef, H.S., 2011. Glycosphingolipids and insulin resistance. *Adv. Exp. Med. Biol.* 721, 99–119. [https://doi.org/10.1007/978-1-4614-0650-1\\_7](https://doi.org/10.1007/978-1-4614-0650-1_7).
- Aji, G., Huang, Y., Ng, M.L., Wang, W., Lan, T., Li, M., Li, Y., Chen, Q., Li, R., Yan, S., Tran, C., Burchfield, J.G., Couttas, T.A., Chen, J., Chung, L.H., Liu, D., Wadham, C., Hogg, P.J., Gao, X., Vadas, M.A., Gamble, J.R., Don, A.S., Xia, P., Qi, Y., 2020. Regulation of hepatic insulin signaling and glucose homeostasis by sphingosine kinase 2. *Proc. Natl. Acad. Sci. U. S. A.* 117 (39), 24434–24442. <https://doi.org/10.1073/pnas.2007856117>.
- Alvarez-Rendon, J.P., Salceda, R., Riesgo-Escovar, J.R., 2018. Drosophila melanogaster as a model for diabetes type 2 progression. *BioMed Res. Int.* 2018, 1417528 <https://doi.org/10.1155/2018/1417528>.
- American Diabetes Association Professional Practice Committee, 2022. 2. Classification and diagnosis of diabetes: standards of medical Care in diabetes-2022. *Diabetes Care* 45 (Suppl. 1), S17–S38. <https://doi.org/10.2337/dc22-S002>.
- Baenas, N., Wagner, A.E., 2022. Drosophila melanogaster as a model organism for obesity and type-2 diabetes mellitus by applying high-sugar and high-fat diets. *Biomolecules* 12 (2). <https://doi.org/10.3390/biom12020307>.
- Bieniasz, K., Fiedorowicz, A., Sadowska, A., Prokopiuk, S., Car, H., 2016. Regulation of sphingomyelin metabolism. *Pharmacol. Rep.* 68 (3), 570–581. <https://doi.org/10.1016/j.pharep.2015.12.008>.
- Chao, X., La, X., Zhang, B., Wang, Z., Li, Y., Bo, Y., Chang, H., Gao, X., Tian, C., Wu, C., Li, J.A., 2022. Sanghuang tongxie formula ameliorates insulin resistance in Drosophila through regulating PI3K/Akt signaling. *Front. Pharmacol.* 13, 874180 <https://doi.org/10.3389/fphar.2022.874180>.
- Chavez, J.A., Summers, S.A., 2012. A ceramide-centric view of insulin resistance. *Cell Metabol.* 15 (5), 585–594. <https://doi.org/10.1016/j.cmet.2012.04.002>.
- Chavez, J.A., Knotts, T.A., Wang, L.P., Li, G., Dobrowsky, R.T., Florant, G.L., Summers, S. A., 2003. A role for ceramide, but not diacylglycerol, in the antagonism of insulin signal transduction by saturated fatty acids. *J. Biol. Chem.* 278 (12), 10297–10303. <https://doi.org/10.1074/jbc.M212307200>.
- Chen, Q., Wang, W., Xia, M.F., Lu, Y.L., Bian, H., Yu, C., Li, X.Y., Vadas, M.A., Gao, X., Lin, H.D., Xia, P., 2021. Identification of circulating sphingosine kinase-related metabolites for prediction of type 2 diabetes. *J. Transl. Med.* 19 (1), 393. <https://doi.org/10.1186/s12967-021-03066-z>.
- Ecker, A., Gonzaga, Tksdn, Seeger, R.L., Santos, M.M.D., Loreto, J.S., Boligon, A.A., Meinerz, D.F., Lugokenski, T.H., Rocha, Jbtid, Barbosa, N.V., 2017. High-sucrose diet induces diabetic-like phenotypes and oxidative stress in Drosophila melanogaster: protective role of Syzygium cumini and Bauhinia forficata. *Biomed. Pharmacother.* 89, 605–616. <https://doi.org/10.1016/j.biopha.2017.02.076>.
- Forbes, J.M., Cooper, M.E., 2013. Mechanisms of diabetic complications. *Physiol. Rev.* 93 (1), 137–188. <https://doi.org/10.1152/physrev.00045.2011>.
- Gallopka, M., Klepsat, P., 2018. Obesity and aging in the Drosophila model. *Int. J. Mol. Sci.* 19 (7) <https://doi.org/10.3390/ijms19071896>.
- Garofalo, R.S., 2002. Genetic analysis of insulin signaling in Drosophila. *Trends Endocrinol. Metabol.* 13 (4), 156–162. [https://doi.org/10.1016/s1043-2760\(01\)00458-3](https://doi.org/10.1016/s1043-2760(01)00458-3).
- Grogan, S., Preuss, C.V., 2023. *Pharmacokinetics. StatPearls. Treasure Island (FL)*.
- Guang, Wei, Ma, Tan Ren Xiang, Nicola, Fuzzati, Sheng, Li Qing, Jean-Luc, Wolfender, Kurt, Hostettmann, 1997. Wahlenbergioside, a phenylpropanoid glucoside from Wahlenbergia marginata. *Phytochemistry* 45 (2), 411–415. [https://doi.org/10.1016/S0031-9422\(96\)00849-7](https://doi.org/10.1016/S0031-9422(96)00849-7).
- Gurgul-Convey, E., 2022. To Be or not to Be: the divergent action and metabolism of sphingosine-1 phosphate in pancreatic beta-cells in response to cytokines and fatty acids. *Int. J. Mol. Sci.* 23 (3) <https://doi.org/10.3390/ijms23031638>.
- Haus, J.M., Kashyap, S.R., Kasumov, T., Zhang, R., Kelly, K.R., Defronzo, R.A., Kirwan, J. P., 2009. Plasma ceramides are elevated in obese subjects with type 2 diabetes and correlate with the severity of insulin resistance. *Diabetes* 58 (2), 337–343. <https://doi.org/10.2337/db08-1228>.
- He, Q., Bo, J., Shen, R., Li, Y., Zhang, Y., Zhang, J., Yang, J., Liu, Y., 2021. S1P signaling pathways in pathogenesis of type 2 diabetes. *J. Diabetes Res.* 2021, 1341750 <https://doi.org/10.1155/2021/1341750>.
- Hong, L., Zha, Y., Wang, C., Qiao, S., An, J., 2021. Folic acid alleviates high glucose and fat-induced pyroptosis via inhibition of the Hippo signal pathway on H9C2 cells. *Front. Mol. Biosci.* 8, 698698 <https://doi.org/10.3389/fmolb.2021.698698>.
- Johnson, A.A., Stolzing, A., 2019. The role of lipid metabolism in aging, lifespan regulation, and age-related disease. *Aging Cell* 18 (6), e13048. <https://doi.org/10.1111/acel.13048>.
- Kamata, S., Oyama, T., Saito, K., Honda, A., Yamamoto, Y., Suda, K., Ishikawa, R., Itoh, T., Watanabe, Y., Shibata, T., Uchida, K., Suematsu, M., Ishii, I., 2020. PPARalpha ligand-binding domain structures with endogenous fatty acids and fibrates. *iScience* 23 (11), 101727. <https://doi.org/10.1016/j.isci.2020.101727>.
- Kayode, O.T., Rotimi, D., Okoh, E., Iyobhebbe, M., Kayode, A.A., Ojo, O.A., 2021. Novel ketogenetic diet formulation improves sucrose-induced insulin resistance in canton strain Drosophila melanogaster. *J. Food Biochem.* 45 (9), e13907 <https://doi.org/10.1111/jfbc.13907>.
- Kim, Hyun-Jun, Dong, Chan Son, Kim, Hyuk-Jin, Choi, Kyung, Oh, Seung-Hwan, Kang, Shin-Ho, 2017. The chemotaxonomic classification of Korean Campanulaceae based on triterpene, sterol, and polyacetylene contents. *Biochem. Systemat. Ecol.* 74, 11–18. <https://doi.org/10.1016/j.bse.2017.07.002>.
- Koyama, T., Texada, M.J., Halberg, K.A., Rewitz, K., 2020. Metabolism and growth adaptation to environmental conditions in Drosophila. *Cell. Mol. Life Sci.* 77 (22), 4523–4551. <https://doi.org/10.1007/s00018-020-03547-2>.
- Lai, M.K., Chew, W.S., Torta, F., Rao, A., Harris, G.L., Chun, J., Herr, D.R., 2016. Biological effects of naturally occurring sphingolipids, uncommon variants, and their analogs. *NeuroMol. Med.* 18 (3), 396–414. <https://doi.org/10.1007/s12017-016-8424-8>.
- Lambert, S.A., Jolma, A., Campitelli, L.F., Das, P.K., Yin, Y., Albu, M., Chen, X., Taipale, J., Hughes, T.R., Weirauch, M.T., 2018. The human transcription factors. *Cell* 172 (4), 650–665. <https://doi.org/10.1016/j.cell.2018.01.029>.
- Lan, Mao, 1959. *Herbal Medicines of Southern Yunnan*. Yunnan People's Publishing House, Kunming.
- Ma, L.X., Wang, Y.Y., Li, X.X., Liu, J.P., 2012. Systematic review on methodology of randomized controlled trials of post-marketing Chinese patent drugs for treatment of type 2 diabetes. *Zhong Xi Yi Jie He Xue Bao* 10 (3), 279–292. <https://doi.org/10.3736/jcim20120306>.
- Marczkowiak, A.R., Zbikowski, A., Zabielski, P., Chlubicz, U., Sadowska, P., Pogodzinska, K., Blachnio-Zabielska, A.U., 2023. The effect of silencing the genes responsible for the level of sphingosine-1-phosphate on the apoptosis of colon cancer cells. *Int. J. Mol. Sci.* 24 (8) <https://doi.org/10.3390/ijms24087197>.
- Maruthur, N.M., Tseng, E., Hutfless, S., Wilson, L.M., Suarez-Cuervo, C., Berger, Z., Chu, Y., Iyoha, E., Segal, J.B., Bolen, S., 2016. Diabetes medications as monotherapy or metformin-based combination therapy for type 2 diabetes: a systematic review and meta-analysis. *Ann. Intern. Med.* 164 (11), 740–751. <https://doi.org/10.7326/M15-2650>.
- Meshrif, W.S., El Husseiny, I.M., Elbrense, H., 2022. Drosophila melanogaster as a low-cost and valuable model for studying type 2 diabetes. *J. Exp. Zool. A Ecol. Integr. Physiol.* 337 (5), 457–466. <https://doi.org/10.1002/jez.2580>.
- Mishra, M., Barik, B.K., 2018. Behavioral teratogenesis in Drosophila melanogaster. *Methods Mol. Biol.* 1797, 277–298. [https://doi.org/10.1007/978-1-4939-7883-0\\_14](https://doi.org/10.1007/978-1-4939-7883-0_14).
- Nanjan, M.J., Mohammed, M., Prashantha Kumar, B.R., Chandrasekar, M.J.N., 2018. Thiazolidinediones as antidiabetic agents: a critical review. *Bioorg. Chem.* 77, 548–567. <https://doi.org/10.1016/j.bioorg.2018.02.009>.
- Pantoja, M., Fischer, K.A., Ieronimakis, N., Reyes, M., Ruohola-Baker, H., 2013. Genetic elevation of sphingosine 1-phosphate suppresses dystrophic muscle phenotypes in Drosophila. *Development* 140 (1), 136–146. <https://doi.org/10.1242/dev.087791>.
- Papavassiliou, K.A., Papavassiliou, A.G., 2016. Transcription factor drug targets. *J. Cell. Biochem.* 117 (12), 2693–2696. <https://doi.org/10.1002/jcb.25605>.
- Pathak, M., Ojha, H., Tiwari, A.K., Sharma, D., Saini, M., Kakkar, R., 2017. Design, synthesis and biological evaluation of antimalarial activity of new derivatives of 2,4,6-s-triazine. *Chem. Cent. J.* 11 (1), 132. <https://doi.org/10.1186/s13065-017-0362-5>.
- Qiu, Z., Wang, X., Yang, Z., Liao, S., Dong, W., Sun, T., Wu, H., Zhang, Q., Pan, Z., Lam, S. M., Shui, G., Jin, J., 2022. GBA1-dependent membrane glucosylceramide reprogramming promotes liver cancer metastasis via activation of the Wnt/beta-catenin signalling pathway. *Cell Death Dis.* 13 (5), 508. <https://doi.org/10.1038/s41419-022-04968-6>.
- Sang, J., Dhakal, S., Lee, Y., 2021. Cucurbitacin B suppresses hyperglycemia associated with a high sugar diet and promotes sleep in Drosophila melanogaster. *Mol. Cells* 44 (2), 68–78. <https://doi.org/10.14348/molcells.2021.2245>.
- Serlie, M.J., Meijer, A.J., Groener, J.E., Duran, M., Endert, E., Fliers, E., Aerts, J.M., Sauerwein, H.P., 2007. Short-term manipulation of plasma free fatty acids does not change skeletal muscle concentrations of ceramide and glucosylceramide in lean and overweight subjects. *J. Clin. Endocrinol. Metab.* 92 (4), 1524–1529. <https://doi.org/10.1210/jc.2006-2347>.
- State Administration of Traditional Chinese Medicine, 1999. *Chinese Materia Medica*. Shanghai Scientific and Technical Publishers, Shanghai.
- Su, L., Chen, Y., Huang, C., Wu, S., Wang, X., Zhao, X., Xu, Q., Sun, R., Kong, X., Jiang, X., Qiu, X., Huang, X., Wang, M., Wong, P.P., 2023. Targeting Src reactivates pyroptosis to reverse chemoresistance in lung and pancreatic cancer models. *Sci. Transl. Med.* 15 (678), eabl7895 <https://doi.org/10.1126/scitranslmed.abl7895>.
- Sun, H., Saeedi, P., Karuranga, S., Pinkepank, M., Ogurtsova, K., Duncan, B.B., Stein, C., Basit, A., Chan, J.C.N., Mbanya, J.C., Pavkov, M.E., Ramachandran, A., Wild, S.H., James, S., Herman, W.H., Zhang, P., Bommer, C., Kuo, S., Boyko, E.J., Magliano, D. J., 2022. IDF Diabetes Atlas: global, regional and country-level diabetes prevalence estimates for 2021 and projections for 2045. *Diabetes Res. Clin. Pract.* 183, 109119 <https://doi.org/10.1016/j.diabres.2021.109119>.
- Takuwa, Y., Okamoto, Y., Yoshioka, K., Takuwa, N., 2012. Sphingosine-1-phosphate signaling in physiology and diseases. *Biofactors* 38 (5), 329–337. <https://doi.org/10.1002/biof.1030>.

- Tan, R.X., Ma, W.G., Wei, H.X., Zhang, L.X., 1998. Glycosides from Wahlenbergia marginata. *Phytochemistry* 48 (7), 1245–1250. [https://doi.org/10.1016/S0031-9422\(97\)00928-X](https://doi.org/10.1016/S0031-9422(97)00928-X).
- Tang, T.T., Konradi, A.W., Feng, Y., Peng, X., Ma, M., Li, J., Yu, F.X., Guan, K.L., Post, L., 2021. Small molecule inhibitors of TEAD auto-palmitoylation selectively inhibit proliferation and tumor growth of NF2-deficient mesothelioma. *Mol. Cancer Therapeut.* 20 (6), 986–998. <https://doi.org/10.1158/1535-7163.MCT-20-0717>.
- Tennessen, J.M., Barry, W.E., Cox, J., Thummel, C.S., 2014. Methods for studying metabolism in Drosophila. *Methods* 68 (1), 105–115. <https://doi.org/10.1016/jymeth.2014.02.034>.
- Tseng, H.H.L., Vong, C.T., Kwan, Y.W., Lee, S.M., Hoi, M.P.M., 2017. Lysosomal Ca(2+) signaling regulates high glucose-mediated Interleukin-1beta secretion via transcription factor EB in human monocytic cells. *Front. Immunol.* 8, 1161. <https://doi.org/10.3389/fimmu.2017.01161>.
- Umeshappa, C.S., Sole, P., Yamanouchi, J., Mohapatra, S., Surewaard, B.G.J., Garnica, J., Singha, S., Mondal, D., Cortes-Vicente, E., D'Mello, C., Mason, A., Kubes, P., Serra, P., Yang, Y., Santamaría, P., 2022. Re-programming mouse liver-resident invariant natural killer T cells for suppressing hepatic and diabetogenic autoimmunity. *Nat. Commun.* 13 (1), 3279. <https://doi.org/10.1038/s41467-022-30759-w>.
- Xu, L., Li, Y., Dai, Y., Peng, J., 2018. Natural products for the treatment of type 2 diabetes mellitus: pharmacology and mechanisms. *Pharmacol. Res.* 130, 451–465. <https://doi.org/10.1016/j.phrs.2018.01.015>.
- Yang, Q., Gong, Z.J., Zhou, Y., Yuan, J.Q., Cheng, J., Tian, L., Li, S., Lin, X.D., Xu, R., Zhu, Z.R., Mao, C., 2010. Role of Drosophila alkaline ceramidase (Dacer) in Drosophila development and longevity. *Cell. Mol. Life Sci.* 67 (9), 1477–1490. <https://doi.org/10.1007/s00018-010-0260-7>.